AD-A072 765 RENSSELAER POLYTECHNIC INST TROY NY DEPT OF MATHEMAT--ETC F/G 20/1
GENERAL EFFECTS OF CURRENT AND SOUND-SPEED VARIATIONS ON SHORT---ETC(U)
JUL 79 M J JACOBSON, W L SIEGMANN N00014-76-C-0288
UNCLASSIFIED RPI-MATH-125 NL

| OF |
AD
A072765

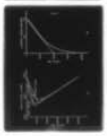

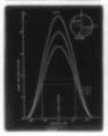

END
DATE
FILMED
9-79
DDC

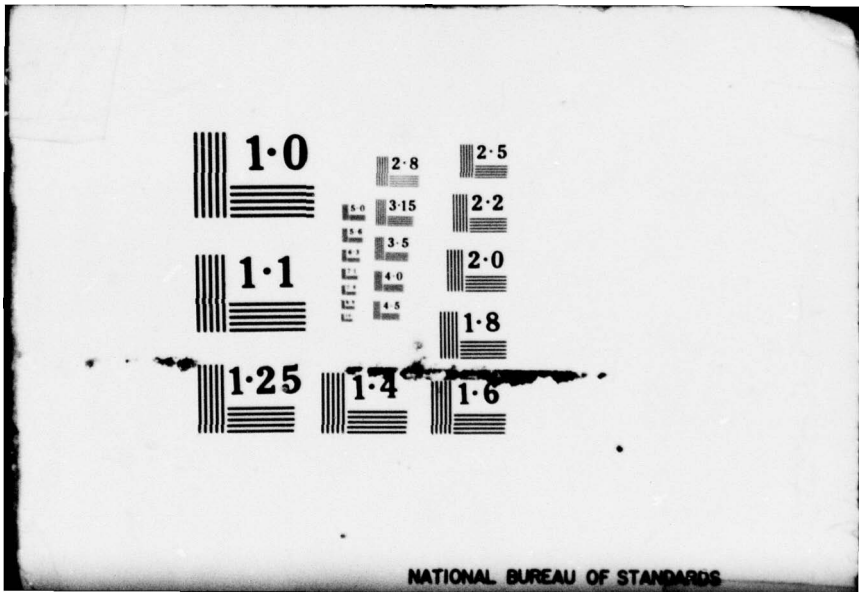
1·0
1·1
1·25
2·8
3·15
3·5
4·0
4·5
2·5
2·2
2·0
1·8
1·4
1·6
NATIONAL BUREAU OF STANDARDS

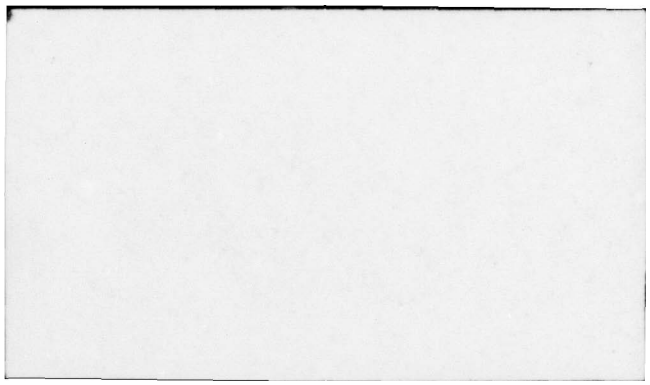

LEVEL II

12

General Effects of Current and Sound-Speed Variations on Short-Range Acoustic Transmission in Cyclonic Eddies

by

M.J. Jacobson, W.L. Siegmann
R.F. Henrick

Department of Mathematical Sciences
Rensselaer Polytechnic Institute
Troy, New York 12181

RPI Math. Rep. No. 125

July 1, 1979

This work was sponsored by
Code 222, Office of Naval Research
Contract No. N 00014-76-C-0288
NR 386-606

ABSTRACT

The effects of sound-speed and current variations induced by a mesoscale cyclonic eddy on short-range propagation are considered. A parametric eddy model is used to determine acoustically-relevant eddy environmental effects, so that eddy-acoustical effects can be determined for eddies of arbitrary size, strength, and position. Approximations to sound-speed and current structures are used to investigate eddy effects on the three-dimensionality of rays and on ray types. The influence of current and sound-speed variations on travel time is examined, and accurate expressions for per-ray phase variation are obtained. Examples are presented illustrating effects of source-receiver position and orientation on per-ray phase shifts and relative phase spreading of arrivals. Also, general results are presented which illustrate the variations of eddy-acoustical effects as functions of source-receiver range and of eddy size and strength.

INTRODUCTION

Recent studies of the mesoscale structure of some mid-ocean regions have shown that eddies are often common-place and long-lasting features.[1] These large rotating bodies of water have been shown to have significant effects on the sound-speed structure of the ocean,[2] primarily resulting from the large temperature deviations associated with eddies. Several analytical studies of the environmental influences of eddies have been carried out, including Refs. 3 and 4. The authors of this paper have presented a model of acoustically-relevant sound-speed perturbations and currents, relating these environmental effects to parameters characterizing eddy size and strength.[5]

Some studies have demonstrated that eddies can have substantial effects on the transmission of sound in the ocean. Nearly all investigators[2,6,7] have assumed two-dimensionality of acoustic rays in studying propagation through a sound-speed structure computed numerically from oceanographic measurements of an eddy. However, Baer[8,9] has considered both two- and three-dimensional parabolic-equation methods to investigate propagation through an eddy, using our model in Ref. 5. Each of the above studies, though, considered only a particular eddy of fixed size and strength, and no investigation was made of the dependence on eddy-acoustical effects of eddy variations. Further, these studies did not consider arbitrary source and receiver orientation with respect to the eddy involved. Moreover, they ignored the effects of the large rotational currents found in eddies, which have been suggested to have possibly significant acoustical effects.[10]

The objective of this paper is to present general results for the influence of ocean eddies of arbitrary size and strength on the transmission of sound. Both currents and sound speed are included, and no restriction is placed on the horizontal location of the acoustic source. In this initial analytical study, however, a short range (<50 km) problem, with both source and receiver on the surface, is considered. Future studies by the authors will permit larger ranges, and other source and receiver depths. In this paper, an investigation of both two- and three-dimensional effects on ray geometry is carried out, and eddy effects on per-ray travel time and phase are determined as functions of eddy parameters and source and receiver position.

In Sec. I, approximations to both eddy currents and sound-speed effects, for use in the acoustical transmission problem, are derived. Using a previously-derived parametric eddy model, these are expressed as simple functions of eddy size and strength. Section II then investigates the effect of eddy sound-speed variations and currents on ray geometry, employing an environmental discretization scheme. The three-dimensionality of rays is examined, and found to be a higher-order effect in short-range problems. The types and variation of rays within an eddy are studied, and ray paths determined for a fixed source and receiver. Section III investigates eddy effects on a transmitted acoustic signal. The principal effects are found to arise through per-ray travel time, and hence phase variation, and analytical expressions are obtained for these quantities. Several examples, relating source and receiver position and orientation within an eddy to per-ray phase variation, are considered in Sec. IV. Also, current

effects are shown to be significant, so that they should not be ignored in eddy-acoustic studies. General results, illustrating the utility of an analytical procedure, are presented for the maximum variation of phase as a function of range and eddy parameters. It is shown that phase variations of over 20 cycles are possible for each ray. Section V summarizes the principal results of the paper.

I. SOUND-SPEED AND CURRENT MODELS

As stated previously, the authors have developed one model for sound-speed and current variations induced by a class of mesoscale eddies.[5] After appropriate non-dimensionalization and scaling of the fluid-dynamical equations, approximate solutions for currents and motion-induced pressure and density perturbations were obtained. Resulting temperature effects were then determined from the Eckart state equation,[11] after which sound speed was found from a modified Wilson's formula.[12] These quantities were taken to be radially symmetric about the eddy center, with horizontally-uniform vertical decay and with dependence on eddy radius, maximum current speed, and depth of influence. The two coordinates of the eddy center completed the parameter set for our model.

To determine sound-speed effects of an eddy of given size and strength, perturbation density and pressure must first be computed from the model equations and used in conjunction with prescribed static density and pressure in the Eckart and Wilson formulas. Typical resulting sound-speed profiles at the eddy

edge and center are shown as the solid curves in Fig. 1(a) for a large cyclonic eddy of radius 125 km and maximum current 100 cm/sec. The principal effects are a decrease in sound speed c within the eddy, resulting from the cold core, and a significant elevation of the SOFAR axis of over 300 m. As a result of the complexity of the Wilson and Eckart formulas, the dependence of these effects on both location within the eddy and model parameters is nonlinear. However, we shall utilize bilinear approximations to the sound-speed structure to simplify both this functional dependence and ray geometry.

Let D denote the uniform depth of the ocean, and z_{As} the SOFAR-axis (minimum sound-speed) depth in the static case - that with the eddy absent. We take the surface and bottom sound speeds equal and denote them by c_o, which will be taken to remain constant with or without the eddy present. The minimum sound speed at the SOFAR axis in the static case is represented by c_{ms}. Specification of D, z_{As}, c_o, and c_{ms} completely determine the bilinear approximation to the static sound speed, as illustrated by the lower dashed curve in Fig. 1(a). In order to model the eddy-induced variations, we first specify a Cartesian coordinate system, centered on the surface at the eddy center. The x and y coordinates lie on the ocean surface, while z is measured positively downward. The SOFAR axis depth at any horizontal position (x,y) is

$$z_A = z_{As} [1 - \delta(r)], \tag{1a}$$

where

$$r^2 = x^2 + y^2 \tag{1b}$$

is radial distance, $\delta(r)$ represents the fractional change in the SOFAR-axis depth, and $\delta(r) = 0$ outside the cylindrical eddy ($r > r_o$). We note from Fig. 1(a) that, below the SOFAR axis, sound-speed variations are minimal, so that the lower sound-speed gradient g_2 is taken to have the constant value

$$g_2 = (c_o - c_{ms})/(D - z_{As}) \ . \tag{2}$$

Variations in sound speed above the axis are represented by a linear profile which pivots on the surface (see Fig. 1(a)), so that the sound-speed minimum c_m is given by

$$c_m = c_{ms} - g_2 \, z_{As} \, \delta(r), \tag{3a}$$

and the corresponding upper-gradient magnitude is

$$g_1 = (c_o - c_m)/z_A \ . \tag{3b}$$

We note that the perturbed sound-speed structure at any point within the eddy is then determined through Eqs. (1) - (3) by specifying $\delta(r)$.

Again, due to the nonlinearity of the Eckart and Wilson formulas, it is not possible to derive a simple analytical form for $\delta(r)$. However, numerical calculations[5] have been made for

static parameters appropriate to the mid-ocean Atlantic region. These have shown that the maximum SOFAR-axis elevation, Δz_{Amax}, can be written as a simple function of the eddy radius r_o and maximum current speed U_o, and is relatively insensitive to the depth of influence of the eddy. From Fig. 9 of Ref. 5, it is seen that this relationship is almost linear in both U_o and r_o, so that we may write

$$\Delta z_{Amax} = 0.028\ U_o\ r_o\ , \tag{4}$$

where U_o is measured in cm/sec, r_o in km, and Δz_{Amax} in m. Further, the model equations show that the sound-speed deviations, and hence the fractional SOFAR-axis elevation $\delta(r)$, have the following properties:

$$\delta(0) = \max \delta(r), \tag{5a}$$

$$\delta(r_o) = 0\ , \tag{5b}$$

and

$$\delta'(0) = \delta'(r_o) = 0\ . \tag{5c}$$

We select the following form for $\delta(r)$ that is motivated by the model equations and matches the solution exactly for small axis elevations:

$$\delta(r) = (\Delta z_{Amax}/z_{As})[J_o(\alpha r/r_o) - J_o(\alpha)][1-J_o(\alpha)]^{-1}. \tag{6}$$

In Eq. (6), J_o is the Bessel function of the first kind of order

zero, and $\alpha \doteq 3.83$ is the first zero of J_1, the Bessel function of the first kind of first order. Equations (1)-(6) completely specify the sound-speed approximations at any point within an eddy of known radius and maximum current speed.

Similar approximations are now made to the current structure within an eddy. The maximum current speed at any horizontal location is at the surface, $z = 0$, and decays monotonically to zero at the maximum depth of eddy influence, $z=z_o$, as illustrated by the solid curve in Fig. 1(b) for a surface current magnitude of 100 cm/sec. Separability of eddy vertical and horizontal structure in the model equations implies that the rate of this decay is identical at any horizontal location, so that only the magnitude S_o of the surface current varies, given from the model equations as

$$S_o(r) = (U_o/m)\ J_1(\alpha r/r_o), \tag{7}$$

where $m \doteq 0.582$ is the maximum value of J_1. We then approximate the vertical current decay from its surface maximum by a linear decrease to zero at the SOFAR axis, while neglecting the small currents below the axis. The resulting expressions for the current components u and v in the x and y directions, respectively, are then linear functions of depth (see Fig. 1(b)), have surface magnitude S_o, and depend on position in the eddy as follows:

$$(u,v) = S_o(r)[(z_A-z)/z_A](-y/r,\ x/r). \tag{8}$$

II. RAY GEOMETRY AND ENVIRONMENTAL DISCRETIZATION

We consider the case of a sound source $\mathcal{S}$ and a receiver $\mathcal{R}$ both on the ocean surface a distance R apart. For convenience, we orient our coordinate system with origin at the eddy center and with x-axis parallel to the source-receiver direction. Using this geometry, the source is located at (x_S, y_S), a distance r_S from the eddy center, and the receiver at (x_R, y_R) with $y_R = y_S$, a distance r_R from the center, as illustrated in Fig. 2(a).

As a result of both eddy currents and horizontal sound-speed variations, an acoustic ray launched from the source and intercepting the receiver will not remain in the vertical plane containing $\mathcal{S}$ and $\mathcal{R}$; rather, it will be a three-dimensional space curve. To examine the deviation out of a vertical plane, we consider a ray launched initially in this plane toward the receiver. One of the modified scalar ray equations proposed by Ugincius[13] describes the deviation $\hat{y}$ from the xz-plane. After discarding lower order effects arising from vertical currents and products of small quantities, this equation simplifies to

$$(c_o c^{-1} \hat{y}')' = z' c_o^{-1} \partial v/\partial z - c_o^{-1} \partial c/\partial y - x' c_o^{-1} \partial u/\partial y , \quad (9)$$

where primes denote differentiation with respect to arc length, and (x', y', z') are the direction cosines of the rays. The terms on the right side of Eq. (9) describe the effects that can cause the rays to become three-dimensional. The first results from the vertical gradient of the current component v perpendicular

to the source-receiver direction. The second is associated with the horizontal sound-speed gradient out of the source-receiver plane, while the third involves the variation of the current component u in the source-receiver direction. Estimates of the maximum magnitudes of these gradients, obtained numerically from figures in Ref. 5, are $|\partial v/\partial z| = O(10^{-3}\ \mathrm{sec}^{-1})$, $|\partial c/\partial y| = O(10^{-4}\mathrm{sec}^{-1})$, and $|\partial u/\partial y| = O(10^{-5}\mathrm{sec}^{-1})$. Thus current effects, represented by the first term on the right of Eq.(9), can be more influential in causing three-dimensional effects than previously studied[9] sound-speed effects.

Equation (9) should be integrated twice, along with two additional equations describing the x- and z- behavior of the rays. However, to the order of terms retained in Eq. (9), it can be shown that it is valid to perform these integrations along the static two-dimensional paths connecting source and receiver. To obtain an upper bound for the excursion $\hat{y}$ of a ray, forms for u, v, and c were obtained from Eqs. (1) - (8), with the use of large, but reasonable, parameter values. For ranges less than 50 km, which are the only ones to be considered in this paper, the deviation $\hat{y}$ was found to be less than 50 m. This leads to a horizontal bearing error of less than 0.01 deg, and an error of less than 0.1 m in total arc length, resulting in insignificant errors in phase. Hence, we will assume that all rays are two-dimensional. For longer ranges, however, deviations out of the xz-plane can be of the order of hundreds of meters, leading to significant bearing errors and phase variations, so that the three-dimensionality of rays cannot necessarily be

neglected. Results for larger source-receiver separations, utilizing horizontal sound-speed variations, have been obtained by Baer.[9] However, only one particular eddy was considered, and eddy currents were not included.

A typical idealized ray from source to receiver is shown in Fig. 2(b). We index this ray by the number N of bottom reflections and/or bottom turning points strictly between $\mathcal{S}$ and $\mathcal{R}$, so that the figure corresponds to an N = 3 ray. We note that, for the short range (R < 50 km) problems considered here, the distance between bottom reflection and/or turning points is small compared to the eddy radius. Thus, little variation in eddy structure is observed over this distance. Therefore, we approximate the eddy sound-speed and current structure by taking average vertical profiles between the source and the first bottom point, between bottom points, and between the last bottom point and the receiver. This partitions the range R into N+1 intervals, as illustrated by the dashed lines in Fig. 2(b), and in each interval, current and sound speed are functions of depth z only. From Eqs. (1) - (8) this discretization can be accomplished by defining the mean values of the fractional SOFAR-axis elevation, δ_i, and the surface current speed in the x direction, V_{oi}, for i = 0,1,...,N. Letting x_i be the i th bottom point for a ray, with $x_o = x_S$ and $x_{N+1} = x_R$ as shown in Fig. 2(b), δ_i and V_{oi} are given by

$$\delta_i = (x_{i+1} - x_i)^{-2} \int_{x_i}^{x_{i+1}} \delta(r)\,dx \qquad (10a)$$

and

$$V_{oi} = -(x_{i+1} - x_i)^{-1} \int_{x_i}^{x_{i+1}} [S_o(r) y_S / r] dx \ . \qquad (10b)$$

We note that the integration is taken on the surface of the ocean, along part of the line connecting the source and receiver, and that the values of x_i for each ray are unknown at this time.

We now consider a ray launched in the xz-plane from the source at an angle θ_{oo} measured positive clockwise from the horizontal. As a result of the horizontal discretization in Eqs. (10), in each interval both the current u in the source-receiver direction and the sound speed c are functions of depth alone, given by Eqs. (2), (3), (8), and (10). For cases of purely depth-dependent sound-speed and current structures, Franchi and Jacobson[14] have shown that the angle θ which the ray makes with the horizontal at any point can be related to the initial launch angle θ_{oo} through a modified Snell's law:

$$c_o^{-1} \cos \theta_{oo} - c_o^{-2} V_{oo} = c^{-1} \cos \theta - c^{-2} u. \qquad (11)$$

The angle θ_{oi} at the surface in interval I_i is given by

$$\cos \theta_{oi} = \cos \theta_{oo} + (V_{oi} - V_{oo}) c_o^{-1}, \qquad (12a)$$

while the angle $\theta = \theta_{bi}$ at the bottom point x_i is given by

$$\cos \theta_{bi} = \cos \theta_{oo} - V_{oo} c_o^{-1} \ . \qquad (12b)$$

If the right side of Eq. (12a) is greater than one in any interval, the ray will not reach the surface, and it becomes what is commonly called a "mixed" ray. Similarly, if the right side of Eq. (12b) is greater than one, the ray will refract before reaching the bottom and also become mixed. However, since the current terms relative to c_o in Eqs. (12) are small, a ray will only become mixed when the initial angle θ_{oo} is small. The largest possible current magnitude in the eddy is the surface maximum U_o. If θ_{oo} is sufficiently large so that

$$\cos \theta_{oo} + U_o c_o^{-1} < 1 \ , \tag{13a}$$

the ray will remain SRBR (surface-reflected/bottom-reflected) at all points within the eddy. For small θ_{oo} and $U_o c_o^{-1}$, this inequality can be approximated by

$$\theta_{oo} > (180/\pi)(U_o c_o^{-1})^{1/2} \ , \tag{13b}$$

where θ_{oo} is measured here in degrees. For a maximum eddy current speed U_o of 150 cm/sec, all rays launched at angles $\theta_{oo} > 3.6^o$ remain SRBR. However, numerical calculations show that, for ranges less than 50 km, all rays that intersect the receiver have a launch angle greater than 6^o and, hence, remain SRBR. We stress that, as range is increased, current-induced mixed rays cannot be neglected, and their existence will greatly influence the received signal.

It has been shown[14] that, when sound-speed and currents are only linear functions of depth, ray paths can be approximated by

circular arcs. In each interval I_i the radius of curvature $R_{ci}^{(1)}$ above the SOFAR axis is

$$R_{ci}^{(1)} = c_o(g_{1i} \cos \theta_{oi} + \nu_i)^{-1} \quad , \tag{14a}$$

and below the axis is

$$R_{ci}^{(2)} = c_o(g_2 \cos \theta_{bi})^{-1} \quad . \tag{14b}$$

In Eq. (14a), g_{1i} is the vertical sound-speed gradient in I_i and ν_i is the vertical current gradient, given by

$$\nu_i = V_{oi}/z_{Ai} \quad , \tag{14c}$$

where z_{Ai} is Eq. (1a) evaluated at $\delta = \delta_i$. Similarly, c_{mi} is the axial sound-speed from Eq. (3a) when $\delta = \delta_i$. In a manner analogous to Ref. 15, it can be shown that the distance d_n to the n th surface reflection, for a ray launched at the angle θ_{oo}, is

$$d_n = \sum_{i=0}^{n} M(i) \left[R_{ci}^{(1)} (\sin \theta_{mi} - \sin \theta_{oi}) + R_{ci}^{(2)} (\sin \theta_{mi} - \sin \theta_{bi})\right] , \tag{15a}$$

where

$$M(i) = \begin{cases} 1 & i = 0, N \\ 2 & i = 1,2,\ldots, N-1 \ . \end{cases} \tag{15b}$$

The angles θ_{oi} and θ_{bi} at the surface and bottom, respectively, are given in Eqs. (12), while the angles θ_{mi} at the SOFAR axis are

$$\cos \theta_{mi} = c_{mi} \, c_o^{-1} \cos \theta_{bi} \tag{16}$$

from Eq. (11). Examples of d_1 and the angles θ_{oi}, θ_{bi}, and θ_{mi} appear in Fig. 2(b).

To determine the launch angle of a ray that intersects the receiver with N bottom reflection points, Eq. (15a) is set equal to the range R. The expressions for $R_{ci}^{(1)}$, θ_{mi}, θ_{oi}, $R_{ci}^{(2)}$, and θ_{bi} from Eqs. (12), (14), and (16) are substituted, and the result is simplified further by using expressions for g_{1i}, z_{Ai}, V_{oi} and c_{mi}. It is then necessary to determine the launch angle θ_{oo} both to completely specify the ray geometry via Eq. (11) and to permit determination of variation of quantities such as spreading loss and bottom and surface phase and amplitude effects. However, the complexity of the resulting equation precludes exact solution for the launch angle θ_{oo}. It is possible to solve for this angle in the static case, θ_{os}, where no currents or horizontal sound-speed variations are present:

$$\tan \theta_{os} = (c_o + c_{ms})(DN)(c_o R)^{-1} - R(c_o - c_{ms})(4Nc_o D)^{-1}. \tag{17a}$$

We then seek an approximation to θ_{oo} by writing

$$\tan \theta_{oo} = \tan \theta_{os} + \gamma. \tag{17b}$$

We note that Eq. (17b) is appropriate when the quantities in Eq. (15a) differ only slightly from their static counterparts. The approximation implied by Eq. (17b) is thus accurate near the eddy edge where the SOFAR-axis elevation remains small. However, near the eddy center, elevations in axial depth occur that are large enough to produce $\delta = O(10^{-1})$, so that significant errors are conceivable in using Eq. (17b).

To avoid this problem, we define a new environmental state, where variations along the transmission range remain small. This "barred" state has no currents or horizontal sound-speed variations. Moreover, the sound-speed structure at all points is identical to that at the source location, with axial depth $\bar{z}_A$ and sound-speed minimum $\bar{c}_m$, given by

$$\bar{z}_A = z_{As}[1-\delta(r_S)] \tag{18a}$$

and

$$\bar{c}_m = c_{ms} - g_2 \, z_{As} \, \delta(r_S). \tag{18b}$$

The barred sound-speed state is an exact representation at the source, and if range is small compared to eddy radius, sound-speed variations over the transmission range are small. The amounts of the variations can again be defined through a fractional axis elevation $\bar{\delta}_i$ in interval I_i. In terms of the $\bar{\delta}_i$, we can express the axial depth and sound-speed minimum at any point as

$$z_{Ai} = \bar{z}_A \, (1- \bar{\delta}_i) \tag{19a}$$

and

$$c_{mi} = \bar{c}_m - g_2 \bar{z}_A \bar{\delta}_i \ , \tag{19b}$$

where $\bar{\delta}_i$ is given by

$$\bar{\delta}_i = [\delta_i - \delta(r_S)][1 - \delta(r_S)]^{-1} \tag{19c}$$

from Eqs. (1a) and (18a).

As deviations from the barred state are small for transmission ranges of interest here, we seek the launch angle θ_{oo} in the form

$$\tan \theta_{oo} = \tan \bar{\theta}_o + \bar{\gamma} \ , \tag{20a}$$

where $\bar{\theta}_o$ is the launch angle in the barred state, given analogously to Eq. (17a) by

$$\tan \bar{\theta}_o = (c_o + \bar{c}_m)(DN)(c_o R)^{-1} - R(c_o - \bar{c}_m)(4c_o ND)^{-1}. \tag{20b}$$

Equation (20a) can be used in Eq. (15a) (with $d_N = R$) to determine the launch angle. Using expressions for currents from Eqs. (7) and (8), as well as the sound-speed deviations from the barred state implied by Eqs. (19), the resulting equation may be simplified. It will then depend only upon ocean parameters and deviations from the barred state, represented by $V_{oi}\, c_o^{-1}$, $\bar{\delta}_i$, and $\bar{\gamma}$. These last quantities are now sufficiently small that squares and products can be neglected, further simplifying the equation for θ_{oo}. After lengthy algebraic simplification, the perturbation to the launch angle is determined in the form

$$\bar{\gamma} = a_1 \sum_{i=0}^{N} M(i)\bar{\delta}(i) + a_2 V_{oo} c_o^{-1} + a_3 \sum_{i=0}^{N} M(i) V_{oi} c_o^{-1}, \quad (21a)$$

where

$$a_1 = \bar{z}_A[\cos(\bar{\theta}_m - \bar{\theta}_o) - 1][2N(D-\bar{z}_A)\cos\bar{\theta}_o(\sin\bar{\theta}_m - \sin\bar{\theta}_o)]^{-1}, \quad (21b)$$

$$a_2 = -[\cos^2\bar{\theta}_o \sin\bar{\theta}_o]^{-1}, \quad (21c)$$

and

$$a_3 = \bar{z}_A(1 - \sin\bar{\theta}_o \sin\bar{\theta}_m)\sin\bar{\theta}_m [2ND\cos^2\bar{\theta}_o \sin\bar{\theta}_o(\sin\bar{\theta}_m - \sin\bar{\theta}_o)]^{-1}$$
$$- \bar{z}_A [2ND(\cos\bar{\theta}_o - \cos\bar{\theta}_m)]^{-1}. \quad (21d)$$

In Eqs. (21), the quantity $\cos\bar{\theta}_m$ is obtained from Snell's Law:

$$\cos\bar{\theta}_m = \bar{c}_m c_o^{-1} \cos\bar{\theta}_o. \quad (21e)$$

The first term on the right in Eq. (21a) results from sound-speed variations from source to receiver, the second from the current at the source, and the third from variations in the current from source to receiver. We note that a_1, a_2, and a_3 are all O(1), so that the correction $\bar{\gamma}$ to the launch angle is of the order of the small parameters $V_{oi}c_o^{-1}$ and $\bar{\delta}_i$.

The magnitude of the angle perturbation $\bar{\gamma}$ depends on the sum of the $\bar{\delta}_i$ and V_{oi}. From Eqs. (10),

$$\sum_{i=0}^{N} M(i)\bar{\delta}_i = \sum_{i=0}^{N} M(i) \left\{(x_{i+1}-x_i)^{-1} \int_{x_i}^{x_{i+1}} \delta(r)dx - \delta(r_S)\right\}[1-\delta(r_S)]^{-1} \quad (22a)$$

and

$$\sum_{i=0}^{N} M(i)V_{oi} = \sum_{i=0}^{N} M(i) \left\{(x_{i+1}-x_i)^{-1} \int_{x_i}^{x_{i+1}} S_o(r) y_S r^{-1} dx\right\}. \quad (22b)$$

The bottom reflection points x_i are still undetermined, since the launch angle θ_{oo} must be known to completely describe the geometry of a ray. However, by examining an equation similar to Eq. (15a) for the location of these points, it can be shown that if the sound-speed, current, and angle terms vary only by terms of $O(\bar{\gamma})$, then the fractional offset $(\bar{x}_i - x_i)/x_i$ is $O(\bar{\gamma})$. Hence, consistent with neglecting products of small parameters in the derivation of Eq. (21a), $x_{i+1} - x_i$ can be replaced by $\bar{x}_{i+1} - \bar{x}_i$. The relationship

$$\bar{x}_{i+1} - \bar{x}_i = M(i)R(2N)^{-1} \tag{23}$$

can then be used to simplify Eqs. (22) to

$$\sum_{i=0}^{N} M(i)\bar{\delta}_i = 2N[1-\delta(r_S)]^{-1}\left\{R^{-1}\int_{x_S}^{x_R}\delta(r)dx - \delta(r_S)\right\} \tag{24a}$$

and

$$\sum_{i=0}^{N} M(i)V_{oi} = 2NR^{-1}\int_{x_S}^{x_R} S_o(r)y_S\, r^{-1}\, dx\ , \tag{24b}$$

where the integration is taken along the surface of the ocean on a line connecting source and receiver.

The correction γ to the static angle, necessary to determine the variation in boundary-interaction effects and spreading loss, can be expressed from Eqs. (17b) and (20a) as

$$\gamma = \tan\bar{\theta}_o - \tan\theta_{os} + \bar{\gamma}\ . \tag{25a}$$

Further simplification is possible using Eqs. (17a) and (20b), resulting in

$$\gamma = \bar{\gamma} + [(c_o - c_{ms})z_{As}][c_o(D - z_{As})]^{-1} \times [DNR^{-1} - R(4ND)^{-1}]\delta(r_s) \ , \qquad (25b)$$

where $\bar{\gamma}$ is given in Eq. (21a). Numerical computations show that for the ranges of under 50 km considered here, the launch-angle variation $\theta_{oo} - \theta_{os}$ is less than one degree. Hence, from Eq. (11), the corresponding angle variation at any other point also satisfies this bound. However, for longer ranges where the launch angle becomes smaller, the presence of sine terms in the denominators of Eqs. (21) could cause much larger angle variations.

The approximate ray geometry is now completely specified for a fixed source and receiver. As a result of the horizontal sound-speed and current discretizations, all rays are approximated by segments of circular arcs. In summary, for short-range problems, we have shown that all rays may be taken to be two-dimensional, and that only SRBR rays intercept the surfaced receiver. These rays are indexed by the number N of bottom reflection points, beginning with the N=1 ray. Through use of the small variation in eddy structure over range, an accurate expression for the launch angle from Eq. (20a) can be obtained for each ray. This is accomplished by calculating $\bar{\theta}_o$ and $\bar{\gamma}$ from Eqs. (20b), (21), and (24). This procedure is valid for arbitrary eddy size and strength, as well as for arbitrary source-receiver orientation and position within the eddy.

III. TRAVEL TIME AND PHASE VARIATION

Specification of all rays connecting source and receiver and their geometries permit determination of travel times. From Ref. 14, travel time T may be computed as

$$T = \int (c+u \cos \theta)^{-1} \, ds, \tag{26}$$

where the integral is taken along the ray path from $\mathscr{S}$ to $\mathscr{R}$. However, Hamilton, Siegmann, and Jacobson[16] have shown that contributions to the travel time due to deviations in ray paths, caused by environmental variations of the order of some small parameter ε, are of higher order, $O(\varepsilon^2)$, than explicit contributions from the integrand. Such an argument has been used[16] to then evaluate Eq. (26) along the known, simpler static path. However, in this study, environmental deviations from the static ocean may be large, of $O(\delta)$, so that significant errors might arise by neglecting squares of these terms. This difficulty may again be avoided by exploiting the "barred" state. As the barred sound-speed state is exact at the source, environmental variations such as currents and sound-speed variations will be small $[O(\bar{\gamma})]$. Consistent with our previous neglect of products of these small parameters, ray path variations can be ignored in evaluating Eq. (26). Consequently, the integral in Eq. (26) may be taken along the corresponding ray path that connects the source and receiver in the barred state, where sound speed is only a function of depth and no currents are present.

Further approximations can also be made to the integrand

in Eq. (26). It is consistent to expand the integrand in the small quantities representing sound-speed variations and currents scaled by the surface sound speed c_o, and to neglect their powers and products. Thereby, Eq. (26) can be simplified to

$$T = \int \{ [\bar{c}(z)]^{-1} - \overline{\Delta c}(x,z) c_o^{-2} - u(x,z) c_o^{-2} \cos \theta_o \} \, ds, \qquad (27a)$$

where the sound speed c has been written as

$$c = \bar{c}(z) + \overline{\Delta c}(x,z). \qquad (27b)$$

In Eqs.(27) $\bar{c}(z)$ is the sound speed at the source, the "barred" state given in Eqs. (2), (3), (6), and (18), and $\overline{\Delta c}(x,z)$ is a convenient representation of sound-speed variation from source to receiver as described in Sec. II.

To determine eddy effects on travel time and phase, it is advantageous to write T as the static travel time T_s plus small eddy-induced fluctuations ΔT:

$$T = T_s + \Delta T. \qquad (28)$$

From Eqs. (26) and (27), ΔT can be expressed as

$$\Delta T = (\bar{T} - T_s) + \Delta T_c + \Delta T_u \ , \qquad (29a)$$

where $\bar{T}$ is the travel time in the barred state,

$$\Delta T_c = -\int \overline{\Delta c}(x,z) c_o^{-2}\, ds \tag{29b}$$

is the contribution from sound-speed variations between source and receiver, and

$$\Delta T_u = -\int u(x,z) c_o^{-2} \cos\theta_o\, ds \tag{29c}$$

results from eddy currents. From Ref. 15 the travel times in the static and barred states can be evaluated as

$$T_s = [2ND(c_o - c_{ms})^{-1}] \log[c_o c_{ms}^{-1} (1+\sin\theta_{ms})(1+\sin\theta_{os})^{-1}] \tag{30a}$$

and

$$\bar{T} = [2ND(c_o - \bar{c}_m)^{-1}] \log[c_o \bar{c}_m^{-1} (1+\sin\bar{\theta}_m)(1+\sin\bar{\theta}_o)^{-1}] , \tag{30b}$$

where log denotes the natural logarithm. The difference $(\bar{T} - T_s)$ in Eq. (29a), representing the variation in travel time between the true static case outside the eddy and the barred state, can be simplified first. Because the magnitudes of $\bar{T}$ and T_s given in Eqs. (30) are very similar, it is most accurate to simplify their difference by first combining the logarithm terms. The resulting expression can then be linearized in parameters characterizing differences in sound speed between the two states divided by c_o. These parameters remain small $[O(10^{-2})]$, although the difference in axial depth, $\delta(r_s)$, can be large $[O(10^{-1})]$. Before writing the final expression for $\bar{T} - T_s$, we turn to the remaining terms in Eq. (29a).

To evaluate the integrals in Eqs. (29b) and (29c), the forms for the sound-speed variations $\overline{\Delta c}$ and currents u from Sec. II are used. The ray paths are connected circular arcs, so that

$$ds = \begin{cases} c_o(\bar{g}_1 \cos \bar{\theta}_o)^{-1} \, d\theta & z \leq \bar{z}_A \\ c_o(g_2 \cos \bar{\theta}_o)^{-1} \, d\theta & z > \bar{z}_A \end{cases}, \tag{31a}$$

and

$$z = \begin{cases} \bar{z}_A(\cos \bar{\theta}_o - \cos \theta)(\cos \bar{\theta}_o - \cos \bar{\theta}_m)^{-1} & z \geq \bar{z}_A \\ \bar{z}_A + (D-\bar{z}_A)(\cos \theta - \cos \bar{\theta}_m)(\cos \bar{\theta}_o - \cos \bar{\theta}_m)^{-1} & z > \bar{z}_A. \end{cases} \tag{31b}$$

From Eqs. (3), (10) and (19), the sound-speed variations $\overline{\Delta c}_i$ and currents $u_i(z)$ in range interval I_i are given approximately by

$$\Delta c_i = \begin{cases} -\bar{g}_1 \, D \, \bar{\delta}_i (D-\bar{z}_A)^{-1} \, z & 0 < z < \bar{z}_A \\ 0 & z > \bar{z}_A \end{cases}, \tag{32a}$$

and

$$u_i = \begin{cases} V_{oi}(\bar{z}_A - z)\bar{z}_A^{-1} & 0 < z < \bar{z}_A \\ 0 & z > \bar{z}_A \end{cases}. \tag{32b}$$

Again, products of terms that will arise in Eqs. (29b) and (29c), such as fractional SOFAR elevation and fractional sound-speed variation, are neglected.

After extensive manipulation of the expressions for $\bar{T} - T_s$ and the integrals in Eqs. (29b) and (29c) [using Eqs. (31) and (32)], the travel-time change ΔT may be written as

$$\Delta T = K_{s1} \, \delta(r_S) + K_{s2}[1-\delta(r_S)] \int_{x_S}^{x_R} V_o(r) c_o^{-1} \, dx + K_{s3} \int_{x_S}^{x_R} [\delta(r) - \delta(r_S)] dx. \tag{33}$$

In Eq. (33), K_{s1}, K_{s2}, and K_{s3} depend only on the static state of the ocean, and may be written as

$$K_{s1} = (2nDz_{As})[c_o(D-z_{As})]^{-1} \left\{ \frac{1 - \cos(\theta_{os} - \theta_{ms})}{(\cos\theta_{os}-\cos\theta_{ms})(\sin\theta_{ms}-\sin\theta_{os})} \right.$$

$$\left. \times [\alpha_1(1+\alpha_1)^{-1}\cos\theta_{os}] + \alpha_2[\alpha_1(1+\alpha_1)^{-1} - \log(1+\alpha_1) + \log(1-\alpha_2) + \alpha_2(1-\alpha_2)^{-1}] \right\}, \tag{34a}$$

$$K_{s2} = -(z_{As}\cos\theta_{os})(Dc_o)^{-1} \left\{ \frac{(\theta_{ms}-\theta_{os})\cos\theta_{os} - (\sin\theta_{ms}-\sin\theta_{os})}{(\cos\theta_{os} - \cos\theta_{ms})(\sin\theta_{ms} - \sin\theta_{os})} \right\}, \tag{34b}$$

and

$$K_{s3} = [z_{As}(c_o-c_{ms})][(D-z_{As})c_o^2]^{-1} \left\{ \frac{\sin\theta_{ms}-\sin\theta_{os}-(\theta_{ms}-\theta_{os})\cos\theta_{ms}}{(\cos\theta_{os}-\cos\theta_{ms})(\sin\theta_{ms}-\sin\theta_{os})} \right\}. \tag{34c}$$

In Eqs. (34)

$$\alpha_1 = R(\cos\theta_{os})(c_o-c_{ms})[2ND(1+\sin\theta_{os})c_o]^{-1} \tag{34d}$$

and

$$\alpha_2 = (c_o-c_{ms})c_o^{-1} . \tag{34e}$$

We note that all of the quantities in Eqs. (34) are determined independent of the size and strength of the eddy and the positions of the source and receiver in the eddy. That is, the coefficients K_{s1}, K_{s2}, and K_{s3} in the per-ray travel-time variation are determined entirely by the transmission range R and the number of bottom reflections N [since θ_{os} and θ_{ms} are determined by these quantities through Eqs. (11) and (17a)]. The size and strength of the eddy,

as well as the orientation of the source and receiver, enter in the determination of ΔT in Eq. (33) solely through the axial variations $\delta(r)$ and the surface currents $V_o(r)$.

The variation ΔT requires computation of integrals of SOFAR axis elevations $\delta(r)$ and surface current components, $V_o(r)$, from the source to receiver. We note that closed-form evaluation of these integrals is impossible, due to the complex form of δ and V_o given in Eqs. (6)-(8). However, we choose to exploit the fact that our range R is small compared to the eddy radius r_o, so that the integrals are approximated by the trapezoidal rule:

$$\int_{x_S}^{x_R} [\delta(r) - \delta(r_S)]dx \doteq R[\delta(r_R) - \delta(r_S)]/2 \tag{35a}$$

and

$$\int_{x_S}^{x_R} V_o(r)c_o^{-1}dx \doteq R[V_o(r_R) + V_o(r_S)]/(2c_o). \tag{35b}$$

Our range assumption also can be used to simplify the forms of K_{s1}, K_{s2}, and K_{s3}. Since all rays are relatively steep, the quantity $\theta_{ms} - \theta_{os}$ is small $[O(10^{-2})]$. By expanding the trigonometric terms in Eqs. (34b) and (34c) in powers of $\theta_{ms}-\theta_{os}$ and discarding higher order terms, it can be shown that

$$K_{s2} \doteq -z_{As}(2Dc_o)^{-1} \tag{36a}$$

and

$$K_{s3} \doteq z_{As}[c_o-c_{ms}][2(D-z_{As})c_o^2\cos\theta_{os}]^{-1} . \tag{36b}$$

These expressions are most accurate for ranges shorter than approximately 30 km, but still represent lowest-order effects for larger ranges. The expression for K_{s1} can also be simplified by considering propagation between a source and receiver both lying on the same diameter, with the source on the eddy edge. As all currents will be perpendicular to an eddy diameter, no current effects enter into the determination of ΔT through Eq. (33). It follows from Eqs. (33) and (35a) that the path reciprocity of travel-time variations if source and receiver positions are reversed implies

$$K_{s1} = R\, K_{s3}. \tag{37}$$

We note that a corresponding expression exists if the trapezoidal rule approximation is not applied, and that Eq. (37) has been approximately verified numerically. Equations (35)-(37) can then be used to simplify Eq. (33) giving

$$\Delta T = \left\{ R z_{As} (c_o - c_{ms}) [2(D - z_{As}) c_o^2 \cos\theta_{os}]^{-1} \right\} [\delta(r_S) + \delta(r_R)]/2$$
$$- R\, z_{As} (2D\, c_o^2)^{-1} [1 - \delta(r_S)]\, [V_o(r_S) + V_o(r_R)]/2 \,. \tag{38}$$

The first term on the right of Eq. (38), corresponding to the sound-speed variation within an eddy, represents the effect of colder water found in a cyclonic eddy, in which a travel time delay will occur. This delay depends only on the the cosine of the initial launch angle (or, equivalently, the transmission range) for any particular ray. Since the cosine decreases with the

number of bottom reflections, larger phase shifts will occur for each successive arrival. Thus, ray arrival times will spread as a result. The second term in Eq. (38) gives the effects of eddy currents on the phase of each ray. For a current component in the same (opposite) direction of propagation, a ray will travel faster (slower), and a negative (positive) travel-time shift will occur. We note that there is no dependence in this term on the number of bottom reflections, so that the current-induced shift is uniform over all rays. This result represents a balance between two effects; specifically, the additional time that rays with more bottom reflections spend in the eddy and are exposed to eddy currents, and the decrease with N of the current component in the ray direction, u cos θ_o.

The preceding determination of travel-time deviations for each ray permits ready construction of per-ray phase shift. We consider an omnidirectional CW source, emitting a signal with frequency f(in Hz). The phase ϕ_N (in cycles) of a ray having N bottom reflections may be written as[15]

$$\phi_N = fT + (N-1)/2 + NS_N \ . \qquad (39)$$

The first term on the right represents the contribution of travel time; the second, that of a π-rad phase shift at each of the N-1 surface reflections; and the third, that of the phase shifts S_N (in cycles)at each of the N bottom reflections. We note that eddy effects are assumed to enter Eq. (39) only through the travel time. This is because the numbers of surface and bottom reflections remain unchanged here, and the bottom phase shift S_N is relatively

insensitive to small changes [$O(\gamma)$] in incident angle, for the steep rays characteristic of a short-range problem. Therefore, the eddy effect on the phase of each ray may be expressed simply as

$$\Delta\phi_N = f\,\Delta T_N \quad , \tag{40}$$

where ΔT_N is the travel-time change from Eq. (38).

The amplitude of each ray A_N can be determined by finding spreading loss and bottom loss per reflection. However, the variation of the ray angles at each bottom reflection and at the receiver have been shown to be small [$O(\gamma)$]. It follows, as in previous investigations,[15] that these effects are of higher-order importance in determining the ray amplitude. Hence, the easily-computed static spreading loss and bottom loss expressions can be used to accurately describe the per-ray amplitude.

If desired, the amplitude A and phase Φ of the total acoustic field at the receiver may be found[15] from the sum of all ray arrivals at $\mathcal{R}$, each of which has an amplitude A_N and phase ϕ_N. However, in mid-ocean regions, clay-silt bottom conditions most often prevail,[17] which have been shown to lead to high bottom losses for the steep angles characteristic of short range problems.[18,19] Under such "lossy" bottom conditions, the amplitude of each ray decreases rapidly with the number of bottom reflections, so that the N=1 ray constitutes the principal contribution to the total acoustic field. It is then possible to approximate the total-field amplitude A by the amplitude A_1 of the first ray, so that

little variation in A will occur. The total-field phase Φ can also be approximated accurately by the phase ϕ_1 of the N=1 ray, so that variations in total-field phase can be determined from Eqs. (39) and (38) with N=1. We do stress, however, that if a less lossy bottom is assumed, it is necessary to consider the effects of additional rays. In such a case, the phase spreading of consecutive arrivals may lead to large total-field amplitude and phase fluctuations, often characteristic of multipath effects.

IV. APPLICATIONS

We now discuss application of the results of our preceding theory to some particular types of sound transmission problems. We stress the generality of these results. This generality will be a consequence of our analytic treatments of eddy current and sound-speed effects for arbitrary eddy radius r_o, maximum current speed U_o, range R, and source and receiver position and orientation, given by (x_S, y_S) and (x_R, y_R). From Eqs. (6) - (8), (17a), (38), and (40), the explicit dependence of the change $\Delta\phi_N$ of phase (in cycles) for the N th ray, due to the presence of an eddy, is

$$\Delta\phi_N = f\Big\{ B_1 U_o r_o (R^2 + B_2^2 N^2 + B_3^2 R^4 N^{-2} + 2R^2 B_2 B_3)^{1/2}$$

$$\times [J_o(\alpha r_S/r_o) + J_o(\alpha r_R/r_o) - 2J_o(\alpha)]$$

$$+ B_4 R U_o [J_1(\alpha r_S/r_o) y_S r_S^{-1} + J_1(\alpha r_R/r_o) y_R r_R^{-1}]$$

$$\times \{1 - B_5 U_o r_o [J_o(\alpha r_S/r_o) - J_o(\alpha)]\}\Big\} , \qquad (41a)$$

where

$$r_S^2 = x_S^2 + y_S^2 \tag{41b}$$

and

$$r_R^2 = x_R^2 + y_R^2 \ . \tag{41c}$$

In Eq. (41a), the dimensional quantities B_1, B_2, B_3, B_4, and B_5 depend only on static ocean parameters and are given as

$$B_1 = 0.028\ (c_o - c_{ms}) \left\{ 2\ c_o^2 (D - z_{As})[1 - J_o(\alpha)] \right\}^{-1} , \tag{42a}$$

$$B_2 = (c_o + c_{ms}) D\ c_o^{-1} , \tag{42b}$$

$$B_3 = (c_o - c_{ms})(4 c_o D)^{-1} , \tag{42c}$$

$$B_4 = z_{As}\ (2Dmc_o^2)^{-1} , \tag{42d}$$

and

$$B_5 = 0.028\ \ z_{As}[1 - J_o(\alpha)]^{-1} \ . \tag{42e}$$

In Eqs. (41) and (42), currents, sound speeds, depths, and radial distances are measured in units of cm/sec, m/sec, m, and km, respectively. Equations (41a) can then be used to illustrate variation of the phase of each ray, as a function of the parameters characterizing eddy size and strength and source-receiver range, position, and orientation.

It is first necessary to specify the quantities in Eqs. (42) by specifying the static state of the ocean area under consideration. Here, we elect to use representative data taken from the mid-Atlantic ocean, as illustrated by the solid curve in Fig. 1(a).[5] A uniform depth of 5 km, surface sound speed c_o = 1543 m/sec, and a static SOFAR-axis depth z_{As} = 1100 m, with a corresponding sound-speed minimum c_{ms} = 1483 m/sec, reasonably fit the static sound-speed profile, as illustrated by the lower dashed

curve in Fig. 1(a). We also consider a source emitting a CW frequency f =400 Hz. Specification of these values gives numerical values of $B_1 = 6.46 \times 10^{-11}$, $B_2 = 9.82 \times 10^{3}$, $B_3 = 1.94 \times 10^{-6}$, $B_4 = 7.94 \times 10^{-8}$, and $B_5 = 1.81 \times 10^{-5}$. These parameter values will be used for all calculations in this section.

We first investigate the effect of variation of source and receiver position within an eddy. The eddy radius r_o is fixed at 125 km and the maximum current speed U_o at 100 cm/sec, values typical of a Gulf Stream Ring.[1] The maximum SOFAR-axis elevation is obtained from Eq. (4) to be 350 m. Initially, the source and receiver are taken to be outside the eddy, on the ocean surface, separated by a range R = 30 km. The source-receiver line is then moved through the eddy center, perpendicular to an eddy diameter, as illustrated in Fig. 3. Our choice of coordinate system implies that this diameter may be taken in the direction of the y-axis with the receiver moving on the diameter. Such a path could also result from an eddy drifting appropriately across a fixed transmission range. We note that, in following such a path, the receiver will move through the point of maximum sound-speed variation at the eddy center. It will also pass through points of maximum surface currents, at about half a radius above and below the center.

Since eddy radius, maximum current speed, and transmission range are fixed, the only variation of the phase shift of each ray in Eqs. (41) enters via source and receiver position. At each point along the source-receiver path, source and receiver position can be determined, and the per-ray phase shifts

calculated through Eq. (41a). These are illustrated in Fig. 3 for the N=1,2, and 3 rays. Initially, both the source and receiver are outside the eddy, resulting in the static phase, and hence a phase variation of zero. As they move into the eddy, the slower sound speeds in the cold core result in phase increases which reach a maximum at the eddy center. Rays having more bottom reflections spend more time in the eddy, and hence experience a larger phase increase, resulting in the relative spreading of arrivals shown by the vertical distances between curves in Fig. 3. Effects of eddy currents are illustrated by the dashed lines in the figure. For negative (positive) y, below (above) the eddy center, currents are in (opposed to) the direction of propagation, so that a smaller (larger) phase increase occurs. Hence, each phase curve is not symmetric about y = 0, as it would be if currents were neglected. The horizontal dashed lines indicate a maximum difference of about one cycle in phase shift observed at equal distances on either side of the eddy center.

A similar behavior would be observed if the source and receiver were to follow any other chord, not necessarily a diameter, through an eddy. Sound-speed effects would cause the phase shifts of each ray to increase as the source and receiver move toward the center of the eddy, and then decrease after passing the point of closest approach to the center. Currents would increase the amount of phase shift when opposite to the direction of propagation, and decrease the phase shift when flowing from source to receiver. We note that current effects

are represented by the second term on the right side of Eq. (41a). As discussed earlier, the current effects are independent of N, so that this variation is uniform for all rays. However, the magnitudes of current and sound-speed effects will vary with the path of the chord. For example, if the transmission range fails to intersect the eddy center, the maximum observed phase shifts will be smaller.

The orientation of the source and receiver at any point will also influence the observed phase shifts, particularly with respect to current effects. We again fix eddy radius at 125 km and maximum current speed at 100 cm/sec. A receiver is fixed 60 km above the eddy center, and the source is rotated clockwise about the receiver, keeping a fixed range of 30 km, as illustrated in Fig. 4. Thus, only the orientation and radial distance of the source vary. Again, the only information required to calculate eddy-induced phase shift in Eq. (41) is the position of the source and receiver. The resulting phase variation of the N=1 ray is plotted in Fig. 4 as a function of rotation angle β relative to the arbitrary initial orientation described by $\beta=0$. The dashed curve illustrates the effect of sound-speed variations alone. That is, currents are absent, as in the case of previous eddy-acoustics studies. The behavior of the curve illustrates the initial motion of the source into an area of lower sound speed, towards the eddy center, resulting in larger (positive) phase shifts. For $\beta > 180^{\circ}$, the source has moved into an area of higher sound speed, toward the eddy edge, resulting in smaller (negative) phase shifts. The larger variations at 90° as compared to 270° occur because higher

sound-speed variations arise moving toward the eddy center than toward the eddy edge.

The solid curve in Fig. 4 illustrates the significant phase variations produced by inclusion of currents. At the arbitrary initial angle $\beta = 0$, currents are entirely in the direction of propagation. As the source is rotated, current components in the source-receiver direction first decrease and then become negative, until at $\beta = 180^{o}$ the current is opposite to the direction of propagation. Initially, the current component at the source increases while that at the receiver decreases, so little variation is noted as β increases to about 30^{o}. Further increases in β result in larger phase variations than would result if, as in previous studies, only sound-speed effects were included. The largest variation occurs at $\beta = 180^{o}$, where an error of one cycle arises if currents are neglected, as shown by the vertical arrow in Fig. 4. This is compared to a total variation of 5 cycles if only sound-speed effects are considered. Again, as indicated by Eq. (41a), current effects will be identical for other rays. At any other location in an eddy, results similar to those in Fig. 4 would be observed. A variation in sound-speed effects would occur as the source moves closer toward or further from the eddy center. Similar current-induced variations would occur as the current component in the source-receiver direction changes with rotation angle. The magnitudes of these effects would vary with the magnitudes of sound-speed variations

and currents, as indicated in Eq. (41a). Both of the examples illustrated in Figs. 3 and 4 clearly indicate the necessity of considering the effects of eddy currents on the phase of an underwater signal.

A principal advantage of an analytical treatment, as opposed to a numerical study, is that general results can be obtained. Thus, through Eqs. (41), the effects on acoustic phase variations of transmission range, eddy radius, and maximum current speed can be examined easily. We choose to discuss effects of these variations on the maximum per-ray phase variation, which results from the large sound-speed variations near the eddy center. Indeed, by examining Eqs. (41) for small source and receiver radii, it can be shown that the largest per-ray phase variation (denoted by $\Delta\Phi_N$) occurs when the source-receiver midpoint is at the eddy center. From Eq. (41a), it follows that

$$\Delta\Phi_N = \omega \left[B_1 U_o r_o (R^2 + B_2^2 N^2 + B_3^2 R^4 N^{-2} + 2R^2 B_2 B_3)^{1/2} \times \{ J_o[\alpha R/(2r_o)] - 2J_o(\alpha) \} \right] . \quad (43)$$

In Eq. (43), there are no current effects, as all currents are perpendicular to the transmission range. We note that the position of the source and the receiver are not unique, since they may lie on any eddy diameter.

We first choose to examine the range dependence of the maximum phase shift for the first 3 rays. The eddy radius and

maximum current speed are again fixed at 125 km and 100 cm/sec, respectively, and the resulting variations with range illustrated in Fig. 5. The phase shift for each ray increases from R = 0, where rays are reflected directly back from the bottom. In this case, the $\Delta\Phi_N$ are predicted from Eq. (43) to be linear functions of N, so the phase shifts of the second and third rays are multiples of 4.8 cycles, the shift of the first. We observe from Fig. 5 the nonlinear growth of the phase shifts with range. Moreover, since this growth changes with N, there is a variation in the relative phase spreading among the rays, indicated by the distances between curves in Fig. 5. For each positive range, the $\Delta\Phi_N$ are nonlinear functions of N so that, as range increases, the relative phase spreading between the second and third rays becomes significantly less than that of the first and second. For example, at 50 km, the phase difference between the N=1 and N=2 (N=2 and N=3) rays is 4.0 (2.3) cycles compared to 3.0 (3.3) cycles at R = 20 km.

At any other point within the eddy, similar effects would occur, although the magnitudes of the phase variations will of course be smaller than the maximum values appearing in Fig. 5. This is because the range-dependent terms in Eq. (41a) are independent of source and receiver position. From Eqs. (41), the current effects at any point are seen to be linear in range R, so that growth of current-induced phase effects will be linear in R. Curves illustrating phase variation with position, such as those in Fig. 3, will thus grow in magnitude with increasing range, although the relative separation will vary as in Fig. 5. Any

asymmetries resulting from current effects will grow linearly with range as well.

A striking feature of a survey of eddy observations, such as Ref. 1, is the variability encountered in size and strength. The acoustical consequences of such variability can be investigated by changing eddy size, described by the radius r_o, and strength, described by U_o. We first fix the eddy radius at 125 km and the transmission range at 30 km, and study the effect of variation of the maximum rotational current speed. From Eq. (43), the maximum phase variation of any ray is a linear function of U_o. This behavior is illustrated in Fig. 6 by both the magnitudes of per-ray phase shifts and relative phase spreading between rays. For example, at U_o = 150 cm/sec, $\Delta\Phi_1$ is 20.2 cycles, which is 1.5 times the value (13.5 cycles) at U_o = 100 cm/sec; similarly, $\Delta\Phi_2$ increases by a factor of 1.5 to 25.3 cycles. At other source-receiver locations within the eddy, similar effects would occur. From Eqs. (41), the per-ray phase shifts resulting from both currents and sound speeds are linear in U_o. Hence, curves illustrating phase variations during an eddy traversal, such as those in Fig. 3, would increase similarly as functions of U_o, in both magnitude and separation.

The effect of eddies of different radii can be investigated similarly, by fixing U_o = 100 cm/sec, R = 30 km, and permitting r_o to vary. The $\Delta\Phi_N$ of the first three rays for radii characteristic of mesoscale eddies, illustrated in Fig. 7, is seen to change significantly with r_o. For example, for the N=2 ray, $\Delta\Phi_2$ changes from 9.4 to 17.2 cycles as r_o increases from 75 to 150 km. From Eq. (43), $\Delta\Phi_N$ depends on r_o both linearly

(as with U_o) and nonlinearly through the Bessel function J_o. However, as shown in Fig. 7 for the first three rays, this nonlinearity is slight, so that the approximation

$$\Delta\Phi_N = \omega \{B_1 U_o r_o (R^2 + B_2^2 N^2 + B_3^2 R^4 N^2 + 2R^2 B_2 B_3)^{1/2} \times [2 - 2 J_o(\alpha)]\} \quad (44)$$

is valid for small $\alpha R/(2r_o)$. We note that this expression depends on quantities such as R and U_o in the same way as Eqs. (41a) and (43), so it could be used to generate graphs such as those in Figs. 4 and 5.

For other source-receiver locations within the eddy, the term in Eq. (41a) due to sound-speed effects would also grow dramatically with increasing eddy radius. In contrast, the current-effect term does not have a corresponding factor of r_o. However, both current and sound-speed effects on per-ray phase depend on the relative radii at the source (r_S/r_o) and receiver (r_R/r_o) in Eqs. (41). Thus, these effects at a fixed position will not be linear functions of r_o. For example, a source that is 75 km away from the center of an eddy with radius of 75 km is at the eddy edge ($r_S/r_o = 1$), where both current and sound-speed effects are absent. On the other hand, in an eddy of radius 150 km, the source will be half-way between eddy edge and center ($r_S/r_o = 0.5$), where currents are near their maxima, and significant sound-speed effects are present. Thus, curves such as those in Fig. 3, illustrating phase variations during an eddy traversal, would vary not only in magnitude and relative

separation but also in horizontal scale as eddy radius varies. In summary, Figs. 5,6, and 7 illustrate the generality of our results, as a consequence of our analytic treatment of eddy environmental and acoustical effects.

V. SUMMARY

This paper represents a general investigation of the effects of mesoscale cyclonic eddies of arbitrary size and strength on relatively short-range underwater sound transmission. Acoustically-relevant environmental effects are determined as functions of eddy radius and maximum current speed, through use of a parametric eddy model which specifies fundamental eddy characteristics (such as SOFAR-axis elevation and surface currents at any horizontal location within an eddy). Pivoting bilinear profiles are used to describe the sound-speed effects of an eddy, and a linear approximation to the current is made.

Ray geometry for a surfaced source and receiver within an eddy is then examined. It is shown that the three-dimensional excursion from the vertical source-receiver plane is sufficiently small that rays may be considered as two-dimensional. Environmental discretization of eddy sound-speed and current effects permits rays to be approximated by a sequence of connected circular arcs, each with a modified radius of curvature. It is shown that, in general, eddy currents can cause surface-reflected/bottom-reflected rays to miss a surface or bottom reflection and become "mixed". However, none of these rays will intersect the receiver for ranges of less than 50 km. An accurate estimate

for the launch angle of all rays intersecting the receiver is then obtained, with effects of both currents and horizontal sound-speed variations included. The geometry of all rays is then completely determined.

The travel time per arrival is expressed as the static travel time plus small changes resulting from eddy effects. These changes consist of terms arising from both sound speed and currents. For the cold-core cyclonic eddies considered here, sound-speed variations result in a phase delay that varies with each ray, so that a relative phase spreading of arrivals is observed. The effects of eddy currents can result in either a phase advance or delay, depending on the current relative to the source-receiver direction. The current effects are virtually independent of the particular rays, so that a uniform shift in phase is observed.

Several examples are considered to illustrate applications of the general theory. A fixed source and receiver separated by 30 km are moved through the eddy, and the resulting phase shifts of the principal arrivals computed. It is observed that both the individual phase shifts and the relative phase spreading of the rays reaches a maximum near the eddy center, where sound-speed perturbations are largest. Current effects alone are shown to produce variations of about one cycle between identical positions above and below the eddy center. This is a significant effect when compared to variations induced by sound speed. The effect of source-receiver orientation within the eddy is considered next. The receiver is fixed within the eddy, and the source rotated in a circular path about the receiver. Neglect of current

effects is shown to lead to an error as large as 20% of the total variation in observed phase. Both of these examples indicate that, in eddy-acoustics problems, it is important to consider current effects, a factor which has been neglected heretofore.

General results are presented for maximum phase fluctuation as a function of transmission range. It is shown that changes in this quantity grow in a nonlinear manner as range increases, but that relative phase spreading is not a monotone function of range. The maximum phase variation is also examined as a function of eddy size and strength, to illustrate the applicability of our general procedure to arbitrary eddies. It is shown that phase fluctuations of over 20 cycles can occur in propagation over a 30 km range within an eddy. These results represent an initial step by the authors in developing general results applicable to arbitrary eddies and to arbitrary source and receiver locations.

REFERENCES

[1]D.Y. Lai and P.L. Richardson, J. Phys. Oceanogr. 7, 670-683 (1977).

[2]A.C. Vastano and G.E. Owens, J.Phys. Oceanogr. 3, 470-477 (1973).

[3]J.C. Andrews and P. Scully-Power, J. Phys. Oceanogr. 6, 756-765 (1976).

[4]G.R. Flierl, J. Phys. Oceanogr. 7, 365-379 (1977).

[5]R.F. Henrick, W.L. Siegmann, and M.J. Jacobson, J. Acoust. Soc. Am. 62, 860-870 (1977).

[6]W. Gemmill and E. Khedouri, "A note on sound ray tracing through a Gulf Stream Eddy in the Sargasso Sea," U.S. Naval Oceanographic Office, Washington DC, NAVOCEANO T.N. 6150-21-74 (1974) (unpublished).

[7]N.L. Weinberg and X. Zabelgogezcoa, J. Acoust. Soc. Am. 62, 888-894 (1977).

[8]R.N. Baer, J. Acoust. Soc. Am. 62S, (A) S29 (1977).

[9]R.N. Baer, J. Acoust. Soc. Am. 63S, (A) S72 (1978).

[10]R.F. Henrick, M.J. Jacobson, W.L. Siegmann, and J.G. Clark, J. Acoust. Soc. Am. 63S, (A) S72 (1978).

[11]C. Eckart, Am. J. Sci. 256, 225-240 (1958).

[12]H.W. Frye and J.D. Pugh, J. Acoust. Soc. Am. 50, 384-386 (1971).

[13]P. Ugincius, J. Acoust. Soc. Am. 37, 476-479 (1965).

[14]E.R. Franchi and M.J. Jacobson, J. Acoust. Soc. Am. 52, 316-331 (1972).

[15]R.N. Baer and M.J. Jacobson, J. Acoust. Soc. Am. 56, 809-816 (1974).

[16]K.G. Hamilton, W.L. Siegmann, and M.J. Jacobson, "Simplified calculation of ray phase variations due to environmental sound-speed and current variations," (in preparation).

[17]A.P. Lisitzin, Sedimentation in the World Ocean (George Banta, Menasha, 1972), pp. 25-29.

[18]K.V. Mackenzie, J. Acoust. Soc. Am. 32, 221-231 (1960).

[19]R.J. Urick, Principles of Underwater Sound (McGraw-Hill, New York, 1967), pp. 130-132.

FIGURE LEGENDS

FIG. 1. (a) Eddy sound-speed effects (solid curves) and bilinear approximations (dashed lines); U_o = 100 cm/sec, r_o = 125 km. (b) An eddy current (solid curve) and linear approximation (dashed line).

FIG. 2. (a) Source and receiver coordinates. (b) Idealized ray, showing reflection points x_i and environmental discretization intervals I_i.

FIG. 3. Phase shifts of first three SRBR arrivals when transmission range varies as shown; U_o = 100 cm/sec, r_o = 125 km, R = 30 km, f = 400 Hz.

FIG. 4. Phase shift of N = 1 ray when transmission range rotates through the angle β as shown. Solid curve indicates currents present; dashed curve neglects currents; U_o = 100 cm/sec, r_o = 125 km, R = 30 km, f = 400 Hz.

FIG. 5. Maximum change in phase of first three arrivals as a function of transmission range; U_o = 100 cm/sec, r_o = 125 km, f = 400 Hz.

FIG. 6. Maximum change in phase of first three arrivals as a function of eddy strength; r_o = 125 km, R = 30 km, f = 400 Hz.

FIG. 7. Maximum change in phase of first three arrivals as a function of eddy radius; U_o = 100 cm/sec, R = 30 km, f = 400 Hz.

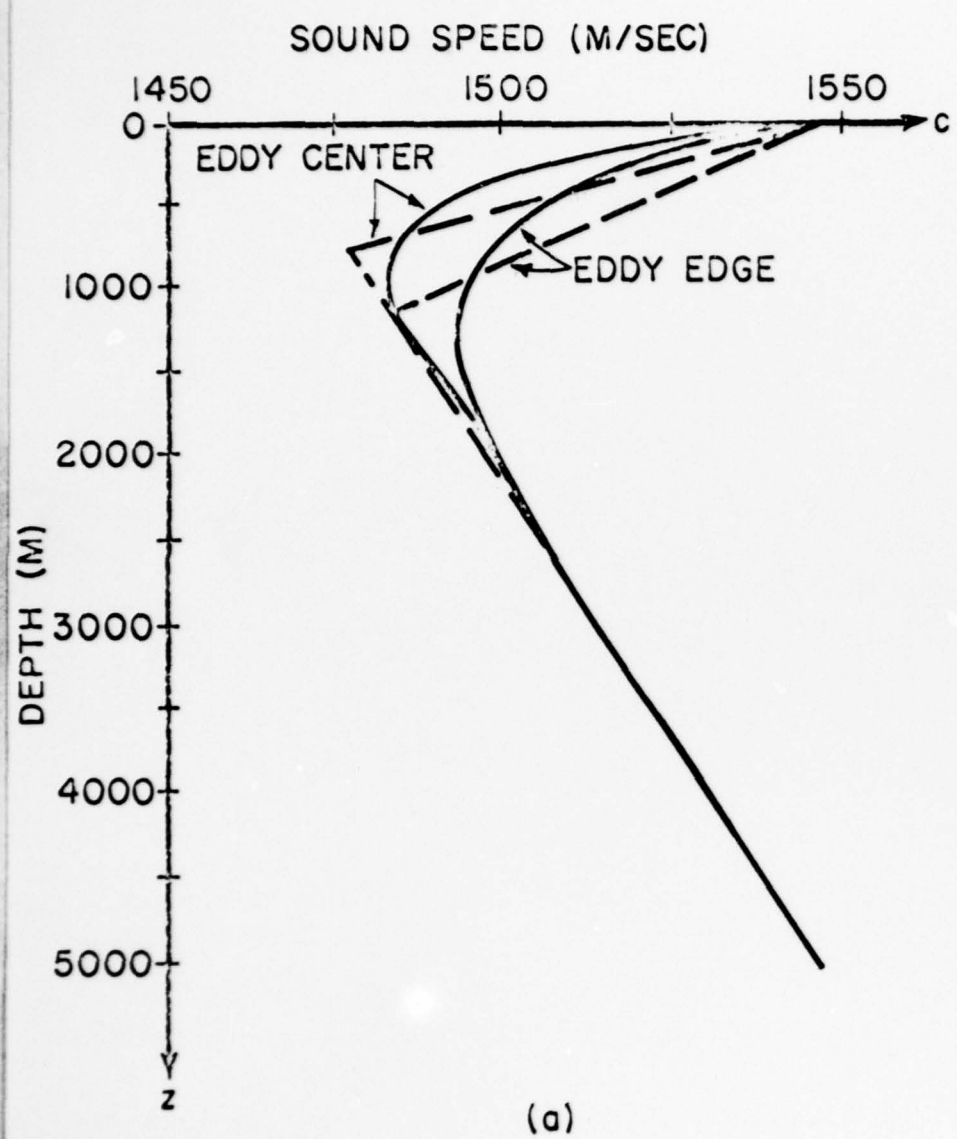
SOUND SPEED (M/SEC)
1450
1500
1550
0
c
EDDY CENTER
EDDY EDGE
1000
2000
3000
4000
5000
DEPTH (M)
z
(a)

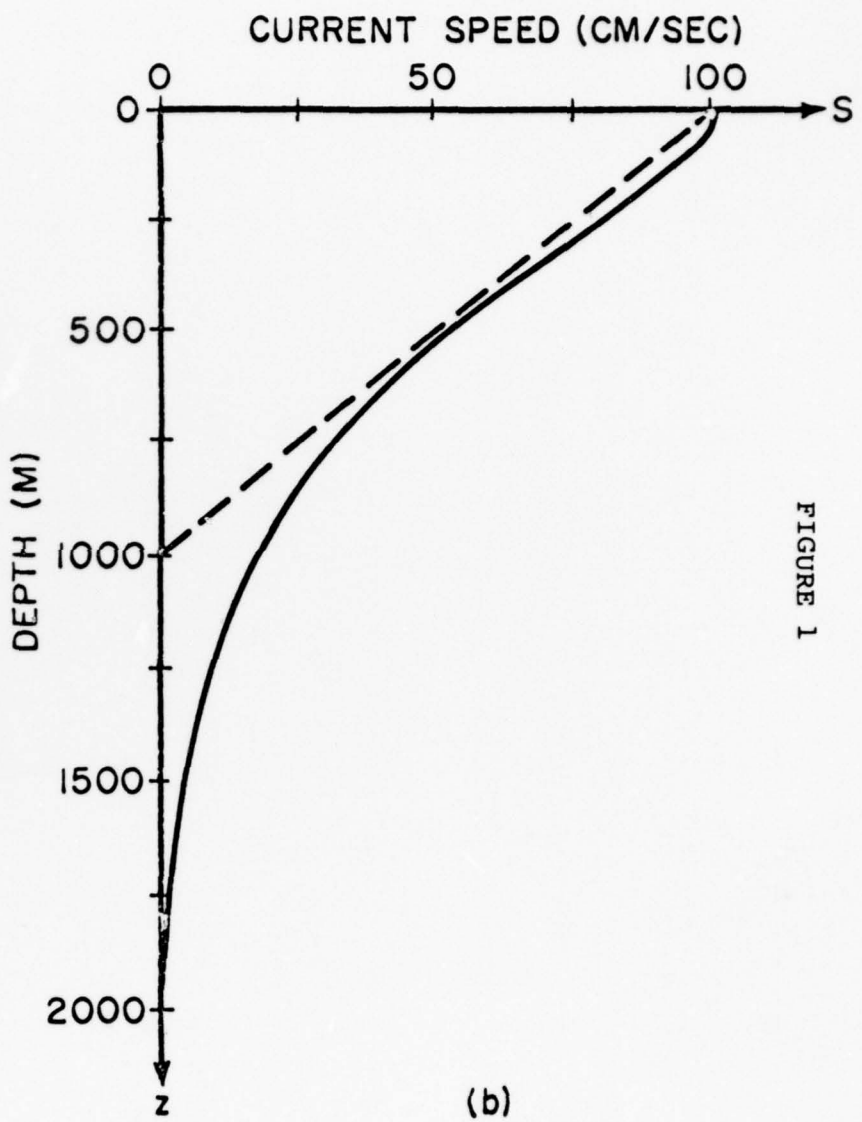
CURRENT SPEED (CM/SEC)
0
50
100
0
S
500
1000
1500
2000
DEPTH (M)
z
(b)

FIGURE 1

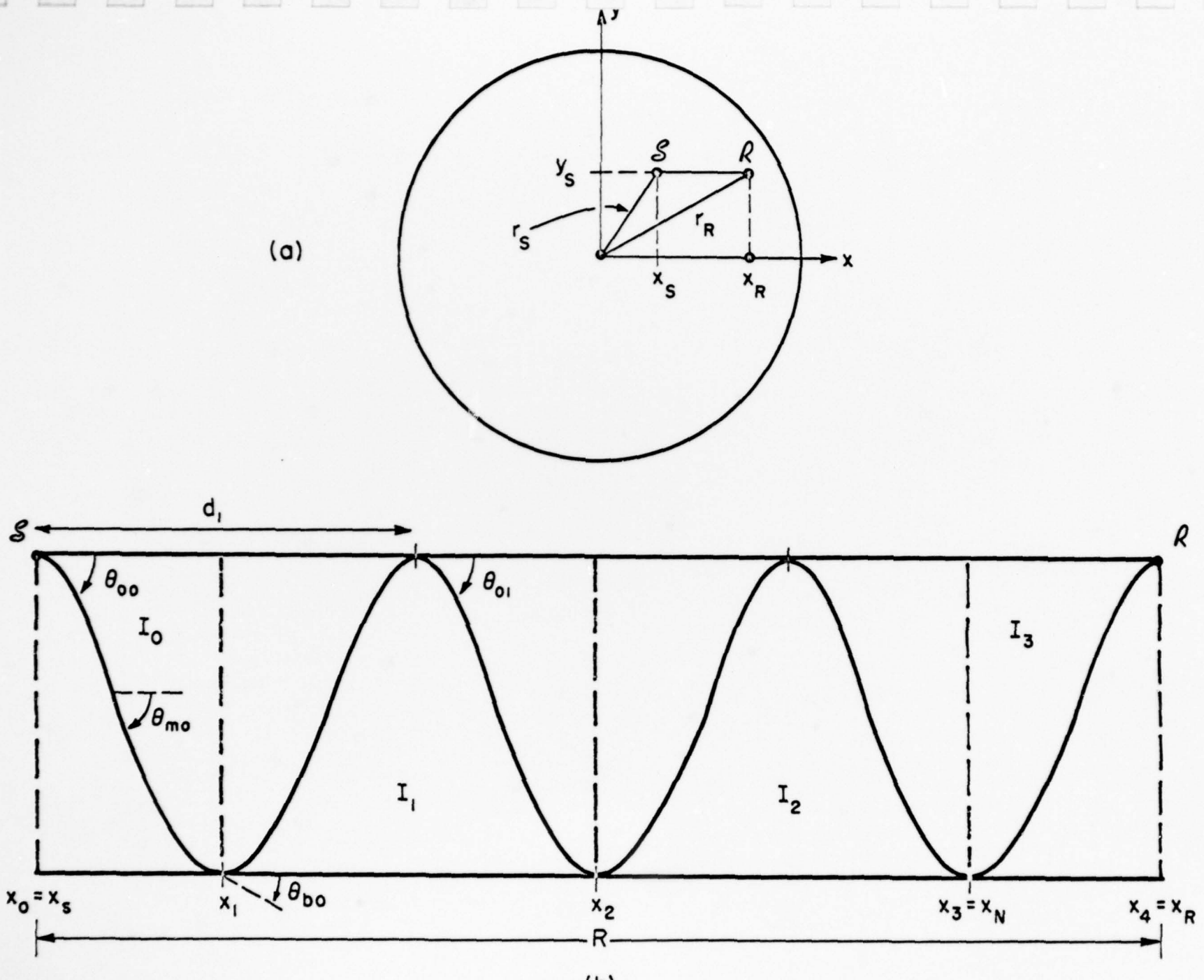
(a)
y
S
R
y_S
r_S
r_R
x
x_S
x_R
d_1
S
R
θ_{00}
θ_{01}
I_0
I_1
I_2
I_3
θ_{mo}
θ_{bo}
$x_0 = x_s$
x_1
x_2
$x_3 = x_N$
$x_4 = x_R$
R
(b)

FIGURE 2

FIGURE 3

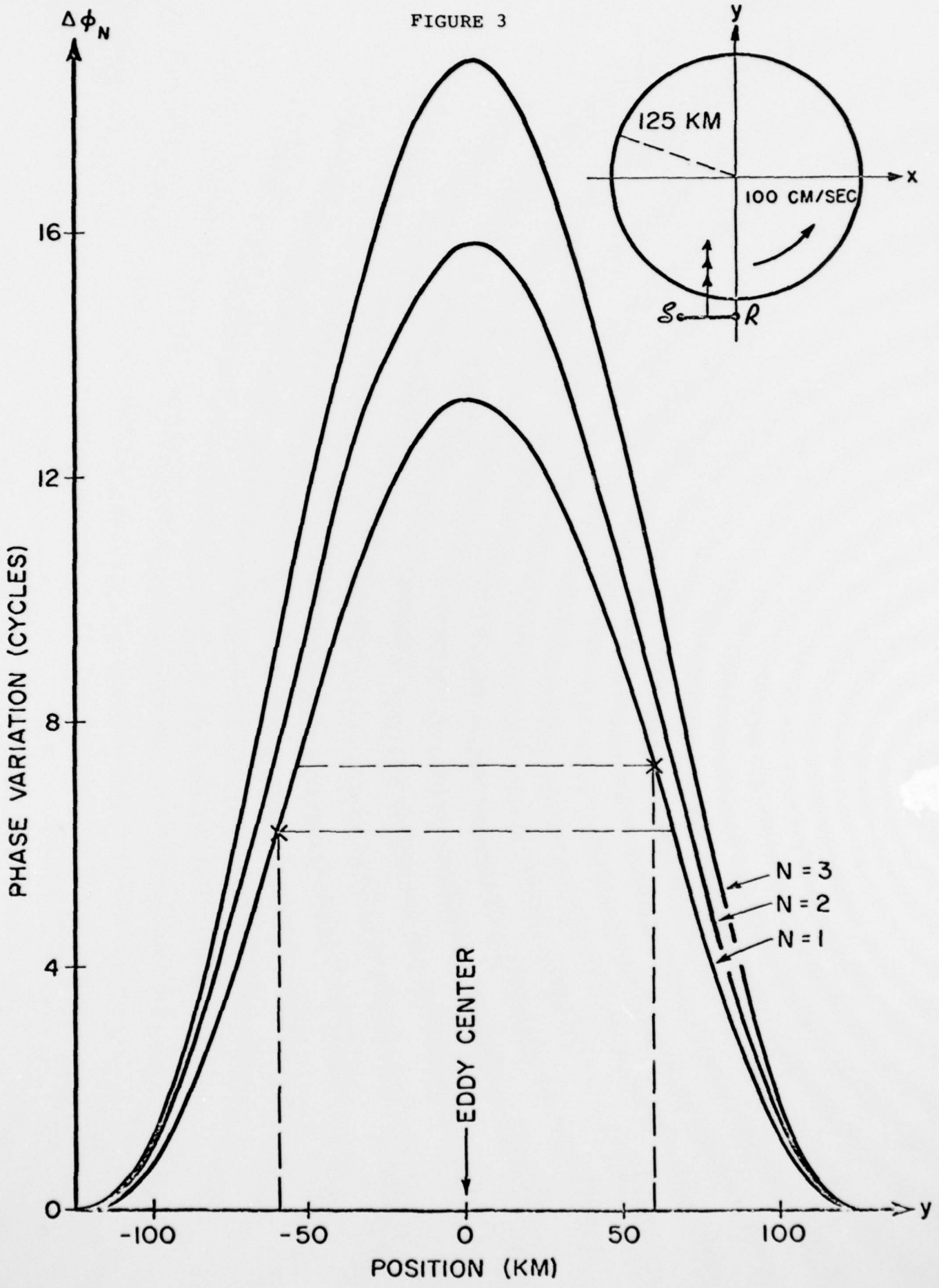
$\Delta\phi_N$
16
12
8
4
0
PHASE VARIATION (CYCLES)
-100
-50
0
50
100
y
POSITION (KM)
EDDY CENTER
N = 3
N = 2
N = 1
y
125 KM
x
100 CM/SEC
S
R

FIGURE 4

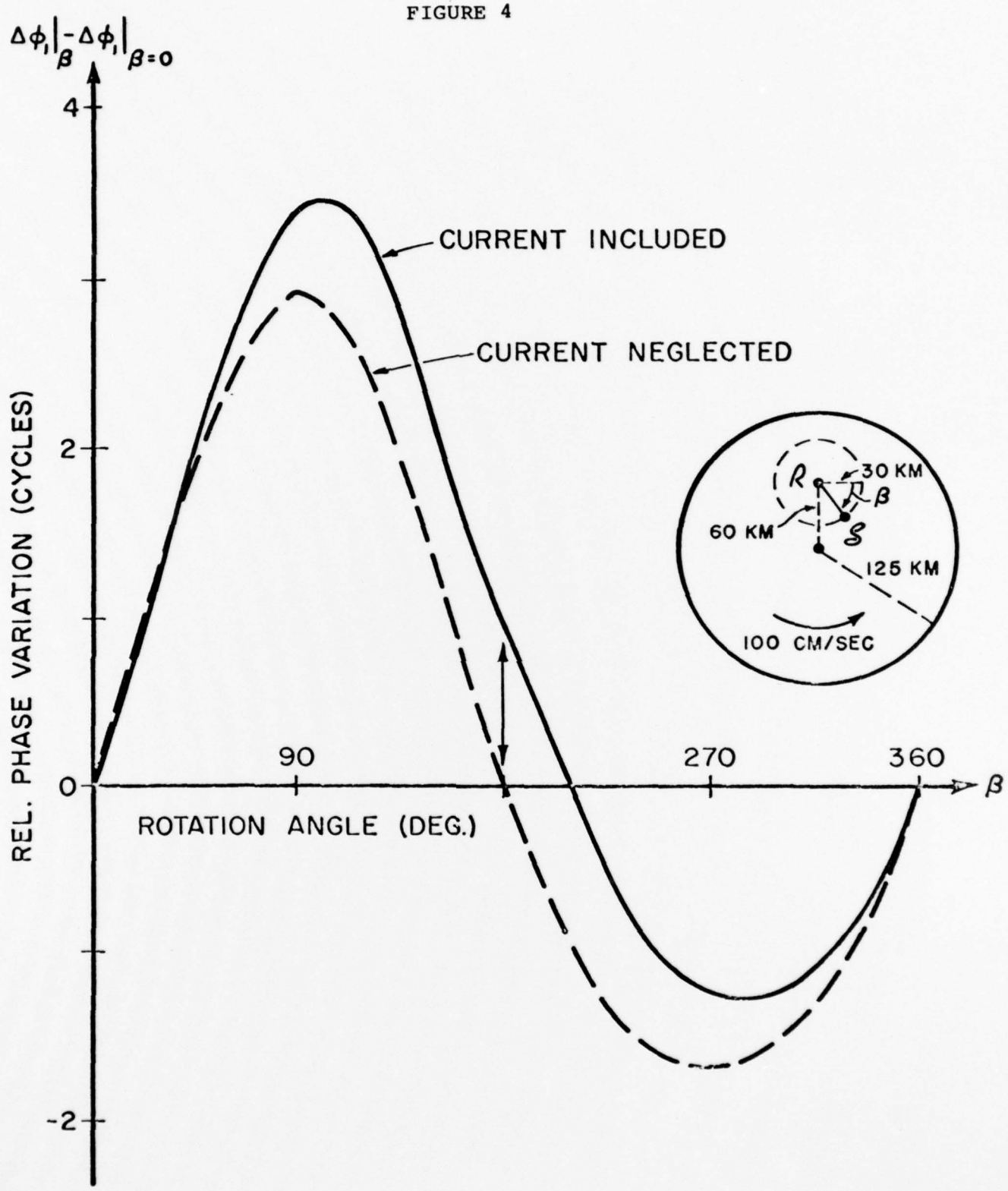
$\Delta\phi_1|_\beta - \Delta\phi_1|_{\beta=0}$
4
2
0
-2
REL. PHASE VARIATION (CYCLES)
CURRENT INCLUDED
CURRENT NEGLECTED
90
270
360
β
ROTATION ANGLE (DEG.)
R
30 KM
β
60 KM
S
125 KM
100 CM/SEC

FIGURE 5

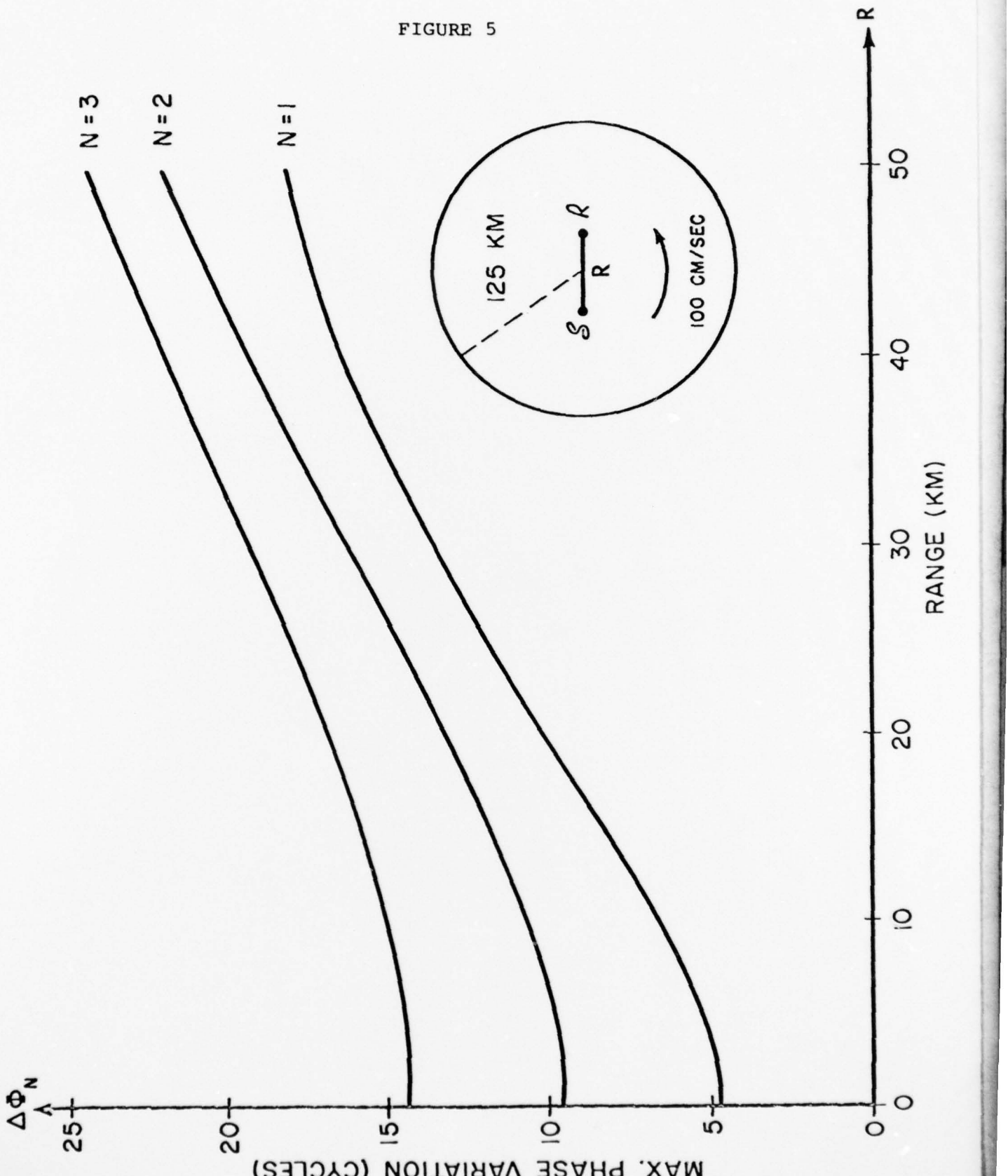
N=3
N=2
N=1
125 KM
S
R
R
100 CM/SEC
$\Delta\Phi_N$
25
20
15
10
5
0
MAX. PHASE VARIATION (CYCLES)
0
10
20
30
40
50
R
RANGE (KM)

FIGURE 6

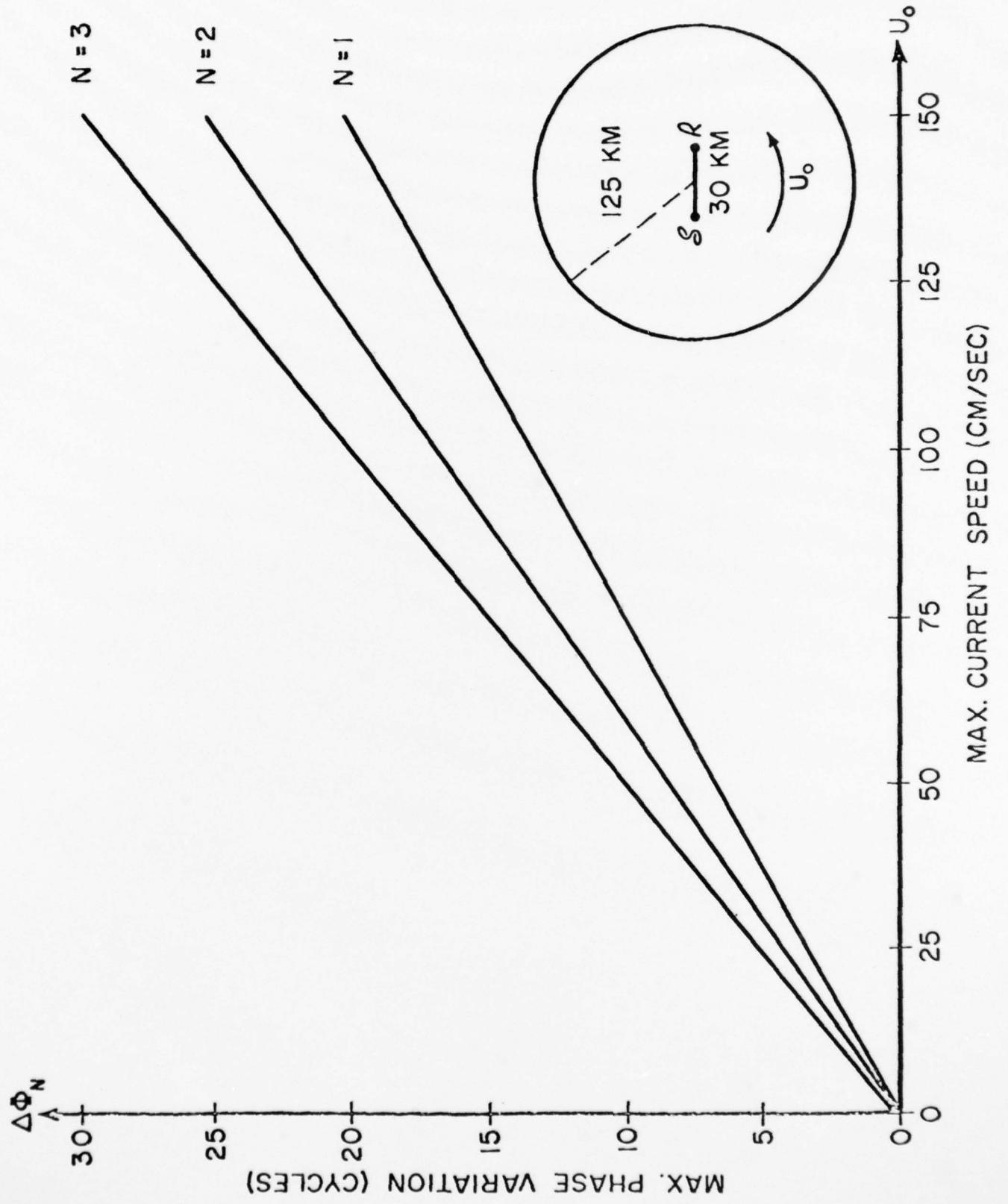
N = 3
N = 2
N = 1
125 KM
30 KM
S
R
U_o
$\Delta\Phi_N$
30
25
20
15
10
5
0
0
25
50
75
100
125
150
U_o
MAX. PHASE VARIATION (CYCLES)
MAX. CURRENT SPEED (CM/SEC)

FIGURE 7

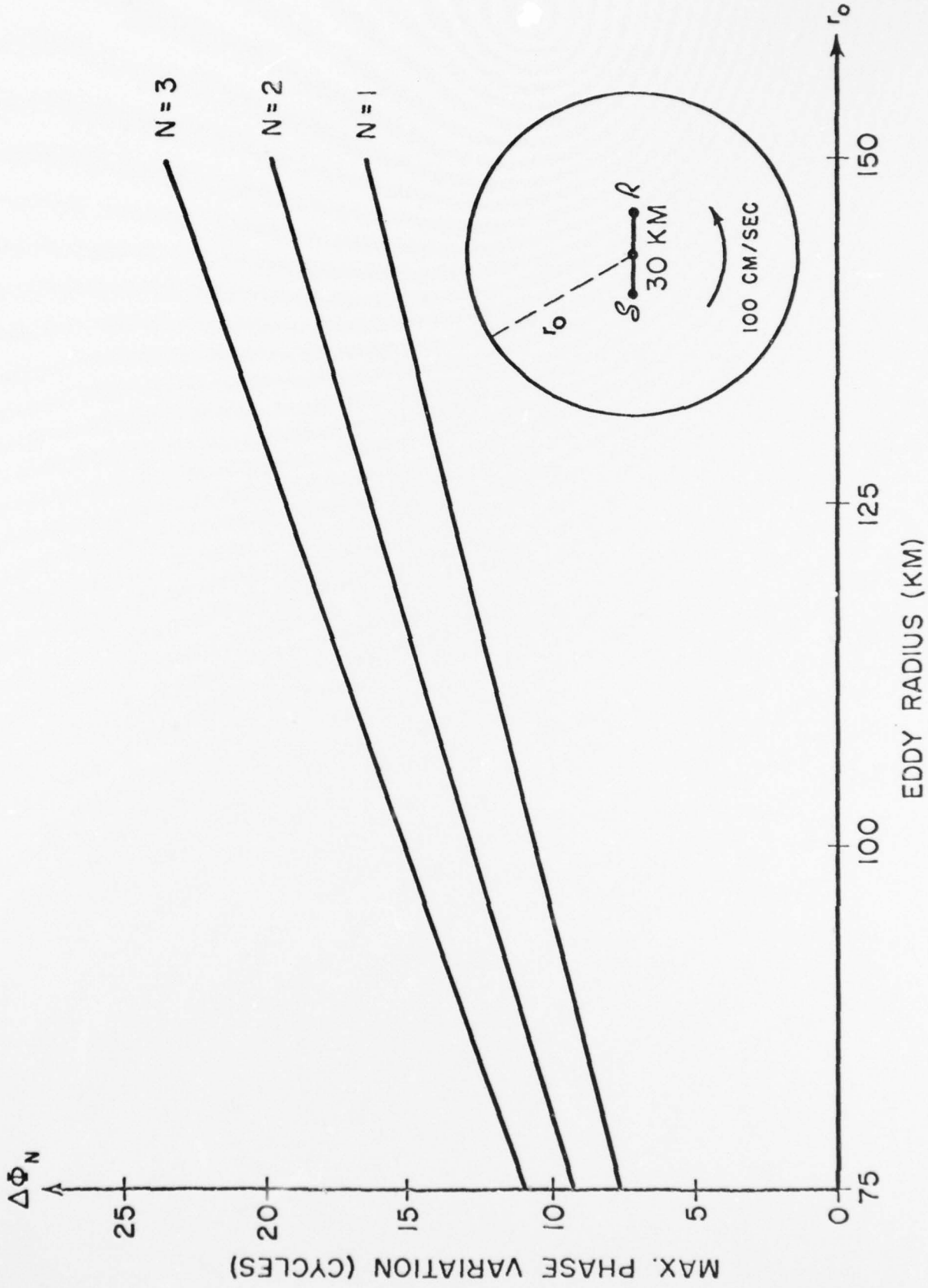
N=3
N=2
N=1
$\Delta\Phi_N$
25
20
15
10
5
0
75
100
125
150
r_o
EDDY RADIUS (KM)
MAX. PHASE VARIATION (CYCLES)
R
S
30 KM
100 CM/SEC
r_o

UNCLASSIFIED
DISTRIBUTION LIST

Addressee	No. of Copies
Office of Naval Research 800 North Quincy Street Arlington, Virginia 22217	
Attn: Code 222	2
102B	1
480	1
486	1
210	1
220	1
Director Naval Research Laboratory 4555 Overlook Avenue, SW. Washington, D.C. 20375	
Attn: Dr. J.P. Dugan	1
Dr. D.R. Palmer	1
Dr. J. C. Munson	1
Mr. R.R. Rojas	1
Dr. B.B. Adams	1
Dr. W.B. Moseley	1
Unclassified Library	1
Superintendent Naval Research Laboratory Underwater Sound Reference Division P.O. Box 8337 Orlando, Florida 32806	1
Director Office of Naval Research Branch Office 1030 East Green Street Pasadena, California 91106	1
Office of Naval Research San Francisco Area Office 760 Market Street, Room 447 San Francisco, California 94102	1
Director Office of Naval Research Branch Office 495 Summer Street Boston, Massachusetts 02210	1
Office of Naval Research New York Area Office 207 West 24th Street New York, New York 10011	1
Commanding Officer Office of Naval Research Branch Office Box 39 FPO New York 09510	1
Director Office of Naval Research Branch Office 536 South Clark Street Chicago, Illinois 60605	1
Office of Naval Research Resident Representative University District Building, Room 422 1107 North East 45th Street Seattle, Washington 98105	1

Addressee	No. of Copies
Technical Director Naval Oceanographic Research and Development Agency NSTL Station Bay St. Louis, Mississippi 39522	
Attn: Dr. Ralph Goodman	1
Mr. E. Smith	1
CDR J.E. Paquin	1
Mr. K.W. Lackie	1
Mr. R. Van Wyckhouse	1
Dr. S.W. Marshall	
Director Naval Oceanographic Office NSTL Station Bay St. Louis, Mississippi 39522	
Attn: Dr. B.E. Olson	1
Dr. T.M. Davis	1
Mr. W.H. Geddes	1
Mr. M.K. Schank	1
Mr. R.A. Peloquin	1
Mr. R. Merrifield	1
Dr. W. Jobst	1
Office of the Assistant Secretary of the Navy for Research, Engineering and Systems Room 4E732, Pentagon Washington, D.C. 20350	1
Chief of Naval Operations Room 4E482, Pentagon Washington, D.C. 20350 Attn: Naval Oceanography Division (OP952)	1
Chief of Naval Operations Room 5D616, Pentagon Washington, D.C. 20350 Attn: Mr. R. Winokur, OP095E	1
Chief of Naval Operations Room 5D580, Pentagon Washington, D.C. 20350 Attn: OP951F	1
Chief of Naval Operations Room 4D518, Pentagon Washington, D.C. 20350 Attn: CAPT J.M. Van Metre	1
Commander Oceanographic System, Atlantic Box 100 Norfolk, Virginia 23511	1
Commander Oceanographic System, Pacific Box 1390 Pearl Harbor, Hawaii 96860	1
Defense Advanced Research Projects Agency 1400 Wilson Boulevard Arlington, Virginia 22209 Attn: Dr. R. Gustafson	1

Addressee	No. of Copies
ARPA Research Center Moffett Field Unit #1 California 94035 Attn: Mr. E. Smith	1
Commanding Officer Fleet Weather Central Box 113 Pearl Harbor, Hawaii 96860 Attn: CDR C. Dunlop	1
Naval Ocean Systems Center (Kaneohe) Kaneohe, Hawaii 96863 Attn: Mr. D. Hightower Mr. B. Kishimoto	1 1
Commander Naval Electronic Systems Command 2511 Jefferson Davis Highway National Center #1 Arlington, Virginia 20360 Attn: CAPT H. Cox, PME 124 CDR D. Griffith, NAVELEX 320	2
Commander Naval Air Systems Command Jefferson Plaza #1 1411 Jefferson Davis Highway Arlington, Virginia 20360	1
Commander Naval Sea Systems Command National Center #2 2521 Jefferson Davis Highway Arlington, Virginia 20362 Attn: SEA 037 Mr. Carey Smith, 06H1 CDR David F. Bolka, 06H2 SEA 003	 1 1 1
Commanding Officer Fleet Numerical Weather Central Monterey, California 93940 Attn: Mr. Paul Stevens Dr. D.R. McLain (NMFS)	1 1
Defense Documentation Center Cameron Station Alexandria, Virginia 22314	12
Director of Navy Laboratories Chief of Naval Material 2211 Jefferson Davis Highway Crystal Plaza #5 Arlington, Virginia 20360 Attn: Dr. James Probus, NAVMAT 08T1 Dr. Tibor Horwath, NAVMAT 08T2	 1 1
Commander Naval Ocean Systems Center Department of the Navy San Diego, California 92132 Attn: Dr. Daniel Andrews Dr. Dean Hanna Mr. Henry Aurand Dr. Harry A. Schenck	 1 1 1 1
Commander Naval Surface Weapons Center Acoustics Division Silver Spring, Maryland 20910 Attn: Dr. Zaka Slawsky	 1

Addressee	No. of Copies
Commander Naval Surface Weapons Center Science and Mathematics Research Group (K05) Dahlgren, Virginia 22448 Attn: Dr. E.W. Schwiderski	 1
Commanding Officer Naval Underwater Systems Center New London Laboratory New London, Connecticut 06320 Attn: Dr. William Von Winkle Dr. A. Nuttall Mr. A. Ellinthorpe Dr. D.M. Viccione Mr. A. Donn Cobb Mr. R. Hasse	 1 1 1 1 1 1
Commander Naval Air Development Center Department of the Navy Warminster, Pennsylvania 18974 Attn: Unclassified Library	 1
Commanding Officer Naval Coastal Systems Laboratory Panama City, Florida 32401 Attn: Unclassified Library	 1
Commanding Officer Naval Underwater Systems Center Newport Laboratory Newport, Rhode Island 02840 Attn: Unclassified Library	 1
Commander Naval Ship Research and Development Center Bethesda, Maryland 20034 Attn: Dr. M. Sevik	 1
Commander David W. Taylor Naval Ship Research and Development Center Bethesda, Maryland 20084	 1
Superintendent Naval Postgraduate School Monterey, California 93940	 1
Superintendent U.S. Naval Academy Annapolis, Maryland 21402 Attn: Library	 1
Commanding Officer Naval Intelligence Support Center 4301 Suitland Road Washington, D.C. 20390 Attn: Dr. Johann Martinek Mr. E. Bissett NISC 34	 1 1 1
Director Applied Physics Laboratory University of Washington 1013 North East 40th Street Seattle, Washington 98105 Attn: Dr. T.E. Ewart Dr. M. Schulkin	 1 1

Addressee	No. of Copies
Applied Research Laboratories University of Texas at Austin P.O. Box 8029 10000 FM Road 1325 Austin, Texas 78712	
Attn: Dr. Loyd Hampton	1
Dr. Charles Wood	1
Institute of Geophysics and Planetary Physics Scripps Institute of Oceanography University of California La Jolla, California 92093	
Attn: Dr. W. Munk	1
Mr. J. Spiesberger	1
Dr. Melvin J. Jacobson Rensselaer Polytechnic Institute Troy, New York 12181	1
Dr. T.G. Birdsall Cooley Electronics Laboratory University of Michigan Ann Arbor, Michigan 48105	1
Dr. M.A. Basin S.D.P. Inc. 15250 Ventura Boulevard Suite 518 Sherman Oaks, California 91403	1
University of Miami Rosenstiel School of Marine and Atmospheric Sciences 4600 Rickenbacker Causeway Miami, Florida 33149	
Attn: Dr. H. Deferrari	1
Dr. W. Duing	1
Dr. David Middleton 127 East 91st Street New York, New York 10028	1
Dr. Donald Tufts University of Rhode Island Department of Electrical Engineering Wakefield, Rhode Island 02881	1
Dr. Loren Nolte Duke University Department of Electrical Engineering Durham, North Carolina 27706	1
Mr. S.W. Autrey Hughes Aircraft Company P.O. Box 3310 Fullerton, California 92634	1
Dr. Thomas W. Ellis Texas Instruments, Inc. 13500 North Central Expressway Dallas, Texas 75231	1
Institute for Acoustical Research Miami Division for the Palisades Geophysical Institute 615 South West 2nd Avenue Miami, Florida 33130	
Attn: Mr. M. Kronengold	1
Dr. J. Clark	1

Addressee	No. of Copies
Mr. Carl Hartdegen Palisades Sofar Station Bermuda Division of Palisades Geophysical Institute FPO New York 09560	1
Mr. Beaumont Buck Polar Research Laboratory 123 Santa Barbara Avenue Santa Barbara, California 93101	1
Dr. M. Weinstein Underwater Systems, Inc. 8121 Georgia Avenue Silver Spring, Maryland 20910	1
Dr. Thomas G. Kincaid General Electric Company P.O. Box 1088 Schenectady, New York 12301	1
Dr. C.N.K. Mooers University of Delaware Newark, Delaware 19711	1
Woods Hole Oceanographic Institution Woods Hole, Massachusetts 02543	
Attn: Dr. Paul McElroy	1
Dr. R. Spindel	1
Dr. John Bouyoucos Hydroacoustics, Inc. 321 Northland Avenue P.O. Box 3818 Rochester, New York 14610	1
Dr. Richard James c/o Fleet Weather Facility 4301 Suitland Road Washington, D.C. 20390	1
Atlantic Oceanographic and Meteorological Laboratories 15 Rickenbacker Causeway Miami, Florida 33149	
Attn: Dr. John Proni	1
Research Triangle Institute Research Triangle Park Durham, North Carolina 27709	
Attn: Dr. E.G. Baxa, Jr.	1
Science Applications, Inc. 8400 Westpark Drive McLean, Virginia 22102	
Attn: Ms. Angela D'Amico	1
Ms. Lorna Blumen	1
Bell Telephone Laboratories 1 Whippany Road Whippany, New Jersey 07981	
Attn: Dr. Bruce Bogart	1
Dr. Peter Hirsch	1
General Electric Company Heavy Military Electronic Systems Syracuse, New York 13201	
Attn: Mr. Don Winfield	1
Jaycor Incorporated 205 South Whiting Street Suite 607 Alexandria, Virginia 22304	
Attn: Dr. S. Adams	1

Unclassified

SECURITY CLASSIFICATION OF THIS PAGE (When Data Entered)

REPORT DOCUMENTATION PAGE		READ INSTRUCTIONS BEFORE COMPLETING FORM
1. REPORT NUMBER RPI Math. Rep. No. 125	2. GOVT ACCESSION NO.	3. RECIPIENT'S CATALOG NUMBER
4. TITLE (and Subtitle) General Effects of Current and Sound-Speed Variations on Short-Range Acoustic Transmission in Cyclonic Eddies		5. TYPE OF REPORT & PERIOD COVERED Technical Report 6. PERFORMING ORG. REPORT NUMBER
7. AUTHOR(s) M.J. Jacobson, W.L. Siegmann, R.F. Henrick		8. CONTRACT OR GRANT NUMBER(s) N 00014-76-C-0288
9. PERFORMING ORGANIZATION NAME AND ADDRESS Rensselaer Polytechnic Institute Troy, New York 12181		10. PROGRAM ELEMENT, PROJECT, TASK AREA & WORK UNIT NUMBERS NR 386-606
11. CONTROLLING OFFICE NAME AND ADDRESS Office of Naval Research, Code 222 Department of the Navy Arlington, Virginia 22217		12. REPORT DATE 1 July 1979 13. NUMBER OF PAGES 53
14. MONITORING AGENCY NAME & ADDRESS(if different from Controlling Office)		15. SECURITY CLASS. (of this report) 15a. DECLASSIFICATION/DOWNGRADING SCHEDULE

16. DISTRIBUTION STATEMENT (of this Report)
This document has been approved for public release and sale; its distribution is unlimited.

17. DISTRIBUTION STATEMENT (of the abstract entered in Block 20, if different from Report)

18. SUPPLEMENTARY NOTES

19. KEY WORDS (Continue on reverse side if necessary and identify by block number)
Underwater Acoustics
Environmental Acoustics
Ocean Eddies

20. ABSTRACT (Continue on reverse side if necessary and identify by block number)
The effects of sound-speed and current variations induced by a mesoscale cyclonic eddy on short-range propagation are considered. A parametric eddy model is used to determine acoustically-relevant eddy environmental effects, so that eddy-acoustical effects can be determined for eddies of arbitrary (over)

DD FORM 1 JAN 73 1473 EDITION OF 1 NOV 65 IS OBSOLETE
S/N 0102-LF-014-6601

Unclassified

SECURITY CLASSIFICATION OF THIS PAGE (When Data Entered)

size, strength, and position. Approximations to sound-speed and current structures are used to investigate eddy effects on the three-dimensionality of rays and on ray types. The influence of current and sound-speed variations on travel time is examined, and accurate expressions for per-ray phase variation are obtained. Examples are presented illustrating effects of source-receiver position and orientation on per-ray phase shifts and relative phase spreading of arrivals. Also, general results are presented which illustrate the variations of eddy-acoustical effects as functions of source-receiver range and of eddy size and strength.